PCP
PLANT & CELL PHYSIOLOGY

Regular Paper

The Alteration of Tomato Chloroplast Vesiculation Positively Affects Whole-Plant Source–Sink Relations and Fruit Metabolism under Stress Conditions

Yoav Ahouvi[1,†], Zechariah Haber[1,†], Yair Yehoshua Zach[1], Leah Rosental[2], David Toubiana[1], Davinder Sharma[1], Saleh Alseekh[3,4], Hiromi Tajima[5], Alisdair R. Fernie[3,4], Yariv Brotman[2], Eduardo Blumwald[5] and Nir Sade[1,*]

[1]School of Plant Sciences and Food Security, Tel Aviv University, P.O.B. 39040, 55 Haim Levanon St., Tel Aviv 6139001, Israel
[2]Department of Life Sciences, Ben-Gurion University of the Negev, P.O.B. 653, 1 David Ben Gurion Blvd., Beer-Sheva 8410501, Israel
[3]Department of Root Biology and Symbiosis, Max Planck Institute of Molecular Plant Physiology, 1 Am Mühlenberg, Golm, Potsdam 14476, Germany
[4]Department of Plant Metabolomics, Center for Plant Systems Biology and Biotechnology, 139 Ruski Blvd., Plovdiv 4000, Bulgaria
[5]Department of Plant Sciences, University of California, 1 Shields Ave., Davis, CA 95616, USA
[†]Equal contribution.

*Corresponding author: E-mail, nirsa@tauex.tau.ac.il

(Received 22 April 2022; Accepted 23 September 2022)

Changes in climate conditions can negatively affect the productivity of crop plants. They can induce chloroplast degradation (senescence), which leads to decreased source capacity, as well as decreased whole-plant carbon/nitrogen assimilation and allocation. The importance, contribution and mechanisms of action regulating source-tissue capacity under stress conditions in tomato (*Solanum lycopersicum*) are not well understood. We hypothesized that delaying chloroplast degradation by altering the activity of the tomato chloroplast vesiculation (CV) under stress would lead to more efficient use of carbon and nitrogen and to higher yields. Tomato CV is upregulated under stress conditions. Specific induction of CV in leaves at the fruit development stage resulted in stress-induced senescence and negatively affected fruit yield, without any positive effects on fruit quality. Clustered Regularly Interspaced Short Palindromic Repeats/CRISPR-associated protein 9 (CRISPR/CAS9) knock-out CV plants, generated using a near-isogenic tomato line with enhanced sink capacity, exhibited stress tolerance at both the vegetative and the reproductive stages, leading to enhanced fruit quantity, quality and harvest index. Detailed metabolic and transcriptomic network analysis of sink tissue revealed that the L-glutamine and L-arginine biosynthesis pathways are associated with stress-response conditions and also identified putative novel genes involved in tomato fruit quality under stress. Our results are the first to demonstrate the feasibility of delayed stress-induced senescence as a stress-tolerance trait in a fleshy fruit crop, to highlight the involvement of the CV pathway in the regulation of source strength under stress and to identify genes and metabolic pathways involved in increased tomato sink capacity under stress conditions.

Keywords: Chloroplast vesiculation • Correlation network analysis • Sink capacity • Source–sink relations • Source capacity • Stress-induced senescence

Introduction

An inherent gap exists between maximal theoretical crop productivity under ideal conditions and actual environment-dependent yield. Closing this gap is a major milestone on the path toward nutritional sustainability. Salinity and water deficit are two factors that contribute greatly to the yield gap: they induce premature senescence in photosynthetic source tissues and reduce plant growth and the number of sink organs by disrupting the movement of assimilated compounds) Munne-Bosch and Alegre 2004). It has been suggested that enhancing photosynthetic capabilities, in order to enhance source capacity, is one of the most important strategies that should be utilized in efforts to meet future global dietary needs under climate change conditions (Zhu et al. 2010, Long et al. 2015).

Climate change negatively affects tomato productivity by modifying the plant source–sink relationships. Therefore, the development of strategies by which tomato plants could maintain both strong source (e.g. photo-assimilation) and sink (e.g. remobilization) capacities, with a delay in stress-induced senescence under water stress and/or irrigation with brackish water (i.e. a water source that is somewhat salty), is highly desirable.

A well-established strategy for enhancing source capacity involves the stay-green trait (Gregersen et al. 2013, Thomas and Ougham 2014). The stay-green trait reflects impaired or delayed chlorophyll degradation. There are two main types of

Plant Cell Physiol. 63(12): 2008–2026 (2022) doi:https://doi.org/10.1093/pcp/pcac133, Advance Access publication on 26 September 2022, available online at https://academic.oup.com/pcp

stay-greens: cosmetic, in which pigment catabolism is the primary lesion, and functional, in which the entire senescence syndrome is delayed or slowed down (Thomas and Howarth 2000). In *Arabidopsis*, there are several characterized pathways that are involved in the degradation of chloroplast proteins such as senescence-associated vacuoles, autophagy and chloroplast vesiculation (CV) (Xie et al. 2015) with autophagy, which have a clear role in stimulating nutrient remobilization upon senescence (Havé et al. 2016, Michaeli et al. 2016). Several studies, mainly in cereals, suggested that breeding for delayed senescence by delaying chloroplast degradation (i.e. the stay-green trait) can improve source capacity throughout stress episodes and improve yield (Gregersen et al. 2013). Chloroplast stabilization increases the ability of source leaves to maintain a high photoassimilation rate and prolongs the overall duration of that assimilation. With regard to the chloroplast degradation pathways (Xie et al. 2015), the CV was shown to be directly involved in stress-induced senescence and to enhance source strength (Wang and Blumwald 2014, Sade et al. 2018b). CV has been previously characterized in *Arabidopsis* and rice, where it was shown to be associated with the chloroplast and involved in the thylakoid membrane and stroma proteins' inactivation by the protein–protein interaction (Wang and Blumwald 2014, Sade et al. 2018b). Consequently, the downregulation of CV in *Arabidopsis* and rice regulated source fitness under stress by delaying chloroplast degradation and enhancing productivity (Wang and Blumwald 2014). Recently, it was demonstrated that delayed senescence (induced by the manipulation of transcription factors) can enhance source capacity, as well as fruit quality and yield, in tomato (Lira et al. 2017, Ma et al. 2018, 2019).

The optimal utilization of enhanced source capacity [i.e. carbon (C) and nitrogen (N) assimilation] requires an effective remobilization of photoassimilates to the sink (i.e. sink capacity). This is of particular importance in fleshy fruits such as tomato, where photoassimilates influence the levels of soluble sugars in the fruit. One established strategy to increase the sink capacity for photoassimilates in tomato is the alteration of fruit cell-wall invertase. The rationale behind this strategy is that the hydrolysis of translocated sucrose at the point of unloading in the fruit sink would increase the translocation gradient from source to sink, increasing the net import of sucrose into the fruits, resulting in higher levels of soluble sugars. A near-isogenic line of tomato, derived from a cross between *Solanum lycopersicum* M82-domesticated tomato and *Solanum pennellii* wild-type (WT) tomato (Eshed and Zamir 1995), with an introgression of fruit-specific cell-wall invertase, exhibited elevated fruit-soluble sugars and sink capacity without any yield effects under optimal conditions (IL9-2-5; Fridman et al. 2004). The major underlying factor leading to increased fruit sugar in IL9-2-5 was an increase in the capacity to take up sucrose unloaded from the phloem (Baxter et al. 2005). Thus, a combination of enhanced source capacity due to the stay-green trait (e.g. CV downregulation) and enhanced sink capacity due to the enhanced loading of sugar into the fruit (e.g. IL9-2-5) can result in improved source–sink interactions, leading to higher tomato yields and improved yield quality under stress conditions.

C and N compounds (represented as metabolites) are assimilated by the plant at the source tissues and are mobilized to the sink tissues. The metabolism of tomato fruits has been widely studied, and several pathways, such as the trichloroacetic acid (TCA) cycle and ethylene metabolism, have been extensively characterized) Nunes-Nesi et al. 2011, Quinet et al. 2019). Abiotic stress affects the primary and secondary metabolism of tomato fruits with negative effects on fruit size and, depending on the stress and its severity, with positive effects on fruit quality (Quinet et al. 2019). Nevertheless, the question of whether and how enhanced source capacity affects sink metabolism in tomato has not yet been fully answered.

CV is conserved within the plant kingdom, with tomato possessing a single *CV* gene (Solyc08G067630). Here, we used a gene-editing technology in a near-isogenic tomato line (IL) of enhanced sink fitness (IL9-2-5, as the genetic background) to study the effect of a stable *cv*-knockout on the quantity and quality of tomatoes grown under abiotic stress. Additionally, we used a parallel approach by which an inducible promoter was utilized to study the effect of the induction of *CV* expression at the reproductive stage on fruit development and quality. We also performed an in-depth analysis of sink-tissue metabolites and transcriptomic data under prolonged abiotic stress and used a machine learning approach to identify unique and novel putative metabolic pathways and genes associated with tomato fruit quality.

Results

Effect of the expression of the *Arabidopsis thaliana CV* gene in tomato

Since the *A. thaliana CV* gene has been well characterized as a stress-induced senescence gene (Wang and Blumwald 2014), a dexamethasone (DEX)-induced *CV* from *A. thaliana* was inserted into the M82 line of tomato. *Arabidopsis thaliana CV* (*AtCV*) expression in the transgenic lines was tested following 4 h of treatment with DEX, and strong gene expression was confirmed (**Fig. 1A**). We used two lines of M82 that contain *AtCV*-inducible genes (L1 and L2). Leaves were sampled from 4- to 5-week-old plants and placed in control solution [H_2O and dimethyl sulfoxide (DMSO)] and in DEX-containing solution for 72 h (**Fig. 1B**). A significant decrease in chlorophyll content (**Fig. 1B**, **C**) was seen when the tissue was placed in the DEX solution, with a considerably more pronounced chlorophyll content decrease in lines L1 and L2 than in the WT.

To further evaluate the effect of *CV*-induced senescence in tomato at the reproductive stage, WT and transgenic plants were grown throughout the entire life cycle until fruit could be harvested. At the early fruit development stage (i.e. a stage by which fruits are at the growth stage and are already active sinks, and nutrient remobilization is active), leaves close to the fruits

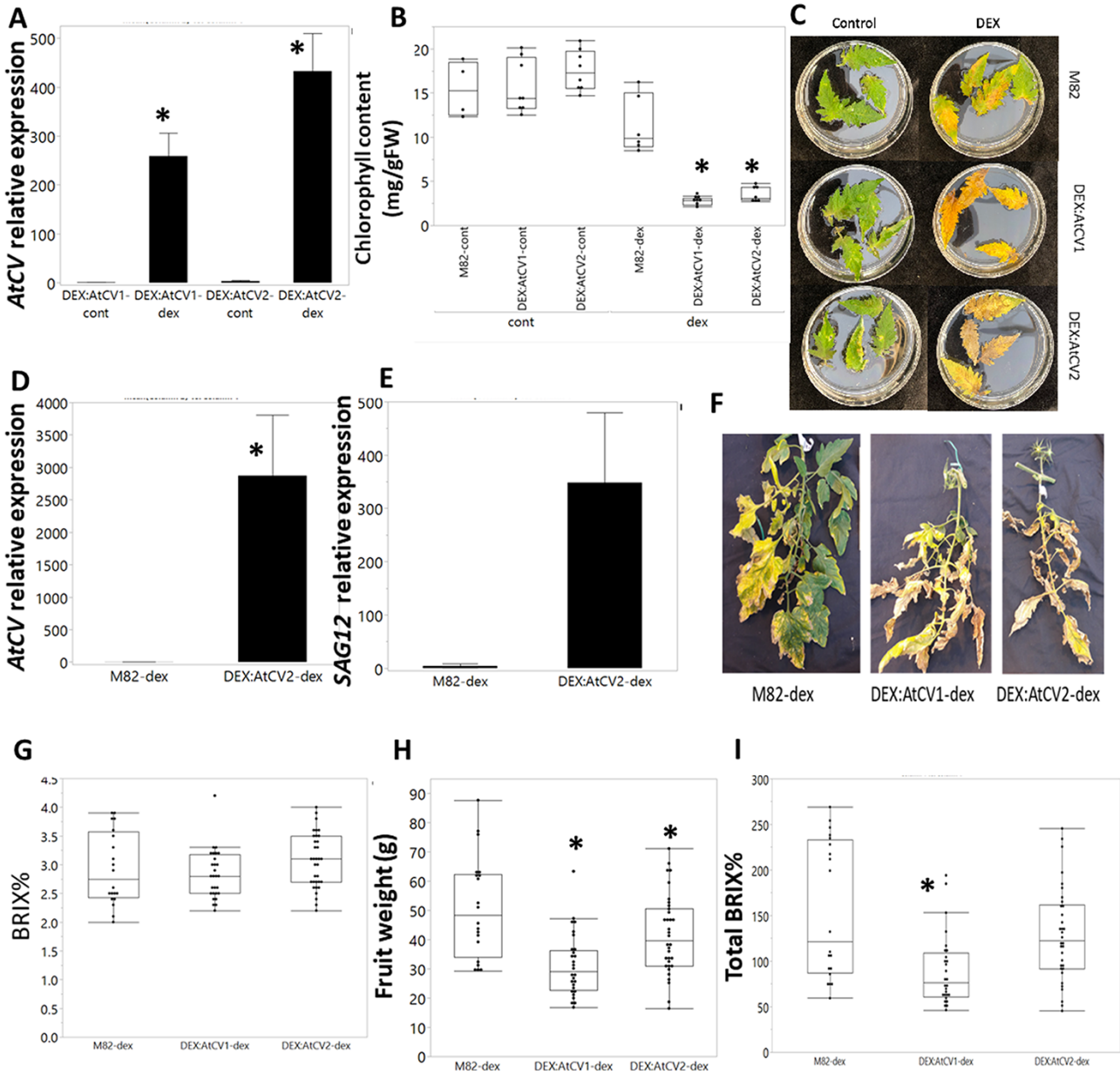

Fig. 1 Phenotypic examination of the effect of expressing *A. thaliana CV* gene in tomatoes. Different phenotypic measurements, taken on tomato lines containing *AtCV* gene fused to a DEX-induced promotor, and WT tomatoes (M82) are presented. 'Cont' stands for control, which were dipped in H_2O and DMSO, and 'DEX' stands for plants that were dipped in DEX solution (50 μM). (A) CV relative expression before treating with DEX and 4 h later. (B) Detached leaves were left floating in DEX solution and were examined for chlorophyll content. (C) Representative detached leaves after DEX solution. (D, E) Relative expression levels of AtCV and SAG12 at the end of the experiment are presented. One leaf from four plants of each group was taken for analysis ($N = 4$). (F) Representative leaves of the lines at fruit harvest time point. (G–I) Brix% levels, average individual fruit weight and product (multiplication) of fruits of WT and DEX:CV-induced plants are presented. Error bars represent the mean ± SE. The boxes represent the interquartile range, the line represents the median and the black dots are all the measurements taken. Asterisk represents significant differences between genotypes and WT ($P < 0.05$, Dunnet's test).

of each plant were routinely dipped in DEX solution to promote *AtCV* expression. *CV* expression in leaves was measured at harvest and found to be significantly higher in the *DEX::CV* line than in the WT (**Fig. 1D**). The expression of *Senescence-Associated Gene 12* (*SAG12*), which encodes a senescence-specific cysteine protease *SAG12* (Gan and Amazino 1995), was also measured and was found to be significantly higher in *DEX::CV* (**Fig. 1E**). DEX treatments additionally enhanced the senescence of the leaves of the transgenic lines, as compared to the DEX-treated WT (**Fig. 1F**).

Yield potential was measured upon treatment with DEX until fruit maturity, in terms of fruit Brix, average individual

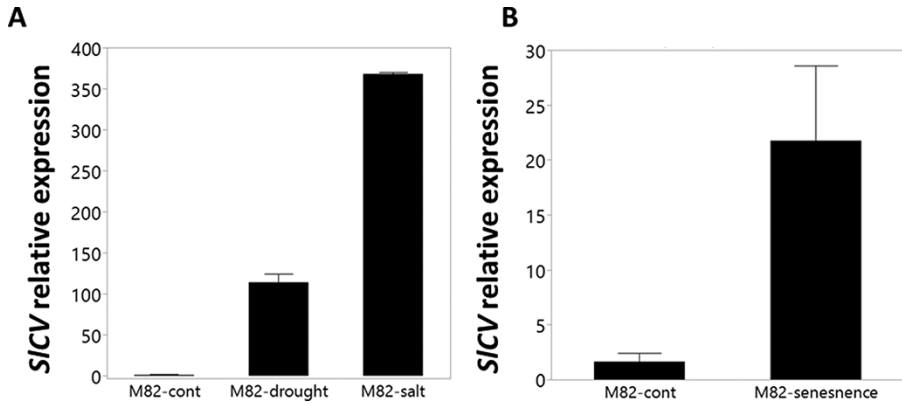

Fig. 2 Tomato CV (SlCV) expression under stress conditions. Three-week-old M82 tomato plants were either well irrigated ('cont', $N = 3$) or exposed to drought (1 week no irrigation—'drought', $N = 3$) or salt (1 week 200 mM NaCl—'salt', $N = 3$). (B) Tomato CV (SlCV) expression in senescence. Leaf samples were taken from a young and viable, well-irrigated plant, 6 weeks old ('cont', $N = 4$) and from an old plant at the end of its reproduction cycle, 12 weeks old ('senescence', $N = 4$). Error bars represent the mean ± SE. Asterisk represents significant differences between genotypes and WT ($P < 0.05$).

fruit weight and total Brix (**Fig. 1G, I**). There was no significant difference between the fruit Brix levels of the WT and *DEX:CV* plants (**Fig. 1G**), although fruit weight was significantly lower among the *DEX::CV* lines (**Fig. 1H**). The product of the multiplication of the average Brix by the fruit weight of each plant (representing total Brix potential) was generally lower in the transgenic lines than in the WT (**Fig. 1I**).

Overall, the results indicate that treating *DEX::CV* lines with DEX caused increased *CV* expression and promoted senescence. As a consequence, the yield was negatively affected without any beneficial effect on fruit Brix.

SlCV expression in tomato during senescence and under stress

We hypothesized that reinforcing the source tissue during abiotic stress, by knocking-out *CV*, could provide a means to generate tomato plants that are able to tolerate stressful, senescence-promoting environments. As a first step to test this hypothesis, we examined the expression of the endogenous tomato *CV* gene under different stress conditions in WT tomato plants. Relative expression of *CV* was examined in leaf samples from 3-week-old well-irrigated WT tomato plants, plants that were exposed to water-deficit stress (1 week without irrigation) or exposed to salt stress (1 week of treatment with 150 mM NaCl). WT tomato plants that were exposed to water-deficit stress or salt treatment exhibited significantly greater *CV* expression, as compared to the well-irrigated plants (**Fig. 2A**).

CV expression in leaves was also examined during the different growth-cycle stages of the plant. The expression of *CV* increased over the course of the plant life cycle, with relatively high expression in leaves of plants at the late fruit stage as compared to the early flowering stage (**Fig. 2B**). These experiments supported the notion that *Solanum lycopersicum CV* (*SlCV*) displayed an expression pattern that was closely related to stress-induced senescence.

Subcellular localization of SlCV protein

To further characterize the tomato CV protein, assessment of its subcellular localization was carried out (Sade et al. 2018b). We used transient agroinfiltration in tobacco leaves, and CV targeting was achieved by using a CV-yellow fluorescent protein (YFP) fusion protein. We found that CV co-localized with the chloroplast, showing a vesicle type pattern that might represent a CV-containing vesicle (CCV) or a CCV aggregation (**Fig. 3**), which was consistent with CV localization using transient expression in *Arabidopsis* and rice (Wang and Blumwald 2014, Sade et al. 2018b).

The effect of tomato *SlCV* expression in *Arabidopsis thaliana*

To assess the possible role of *SlCV* in chloroplast degradation, *SlCV* was expressed under the control of a DEX-inducible promotor in *Arabidopsis*, and two independent transgenic mutants were generated. The mutants were grown and *SlCV* expression was induced with DEX as described in Materials and Methods. quantitative PCR (qPCR) of T_2 generation plants showed that *SlCV* expression increased only in DEX-treated plants (**Fig. 4A**). In these plants, growth was inhibited, chlorophyll levels decreased (**Fig. 4B**) and plant senescence was induced (**Fig. 4C**). This indicated an occurrence of a *CV*-enhanced stress-induced senescence that resulted in a decline of leaf source capacity. WT plants were unaffected by the DEX treatment.

Generation and molecular characterization of CRISPR/Cas9-CV mutants

We used the CRISPR/Cas9 methodology to generate functional knockouts of *SlCV* in IL9-2-5 tomato plants. IL9-2-5 is characterized by an apoplastic invertase with a relatively high affinity for sucrose and relatively high levels of soluble hexoses in the fruit, leading to increased fruit Brix of plants grown

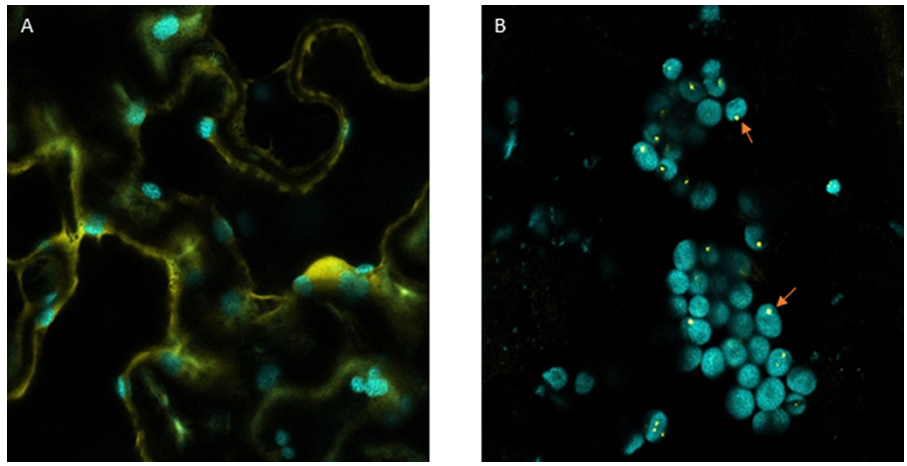

Fig. 3 Tomato CV (SlCV) protein subcellular localization in tobacco using transient agroinfiltration. (A) Free YFP (yellow signal), autofluorescence of chloroplasts (cyan signal). (B) CV-YFP. CV is co-localized with the cell chloroplast (arrows).

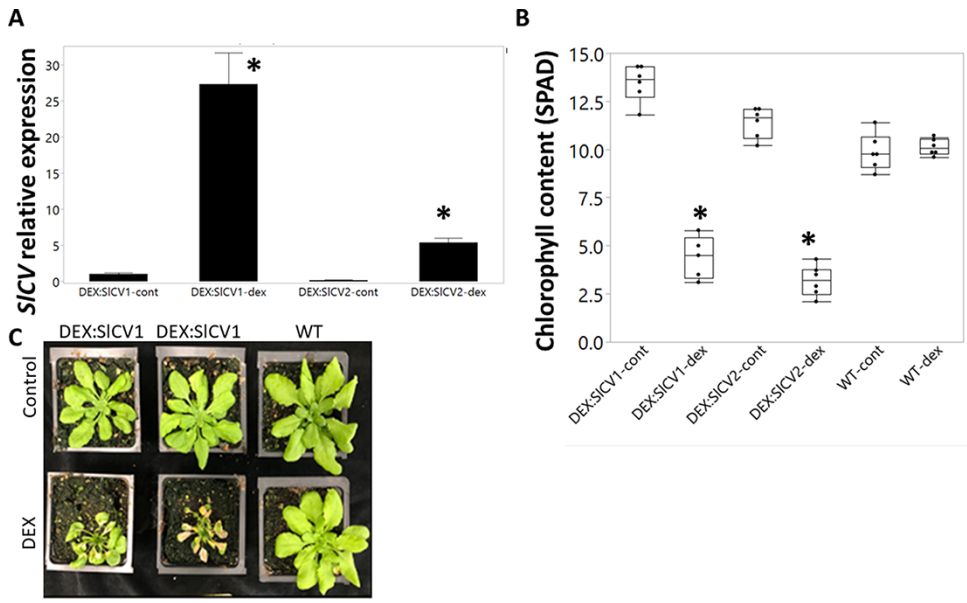

Fig. 4 The effect of tomato CV (SlCV) in *A. thaliana*. Inducing the expression of SlCV in *A. thaliana* inhibits growth and promotes senescence. (A) Phenotypic response in the plants. (B) Control group ('control') and the treatment group ('DEX') were sprayed daily with DEX (50 μM) to induce CV expression. Chlorophyll concentration was measured by SPAD reading. (C) Leaf samples were taken for measuring the relative expression of CV using qPCR. Error bars represent the mean ± SE. The boxes represent the interquartile range, the line represents the median and the black dots are all the measurements taken. Asterisk represents significant differences between genotypes within treatment ($P < 0.05$, *t*-test).

under well-watered conditions and a relatively high sink capacity (Fridman et al. 2002, 2004, Zanor et al. 2009). Because stress-induced senescence had a strong effect on C allocation (Rankenberg et al. 2021), we used a sink-enhanced line as the genetic background (**Supplementary Fig. S1**), based on the assumption that this property might contribute to mitigate the effects of stress and allow for the maintenance of a strong sink and, possibly, a more stable source under abiotic stress.

Screening and selection were performed in seeds of T_0 plants and involved a few steps aimed at the isolation of a Cas9-free homozygous mutant with the *CV* deletion. T_0 plants were characterized for the guide RNA (gRNA) region, and two mutants were found in the gRNA1 region in exon1 (**Supplementary Table S1**). T_1 plants were characterized for mutation homozygosity and scanned for the absence of the transgene cassette. Two homozygous Cas9-free mutants were found, and T_2 seeds were harvested from those mutants.

The two mutants were identified and used for the rest of this study, hereafter named CRISPR-1 and CRISPR-2 (**Fig. 6B**, **C**), both harboring a 2-bp and 4-bp deletion and resulting in a frameshift mutation and stop codon, respectively, as well as a

Fig. 5 The generation of CV tomato knockout lines using CRISPR/CAS9. (A) Schematic representation of the SlCV locus with exons indicated in gray. The sites targeted by sgRNA1 are indicated. (B) Nucleotide sequences of the cv mutants (CRISPR 1 and CRISPR2) and the parental sequence. The regions deleted are highlighted in dashed lines. (C) The predicted amino acid sequences of the mutant alleles. The mutations generated frameshifts that resulted in missense mutations and early stop codons.

non-functional CV protein. The low Cutting Frequency Determination off-target score, according to CRISPOR (Concordet and Haeussler 2018), suggested that the sgRNA1 did not target any gene other than *CV* (**Supplementary Fig. S2**). This computational prediction was validated using PCR and sequencing, further confirming that there were no off-target genes of the sgRNA1 (**Supplementary Fig. S2**).

Phenotypic characterization of responses to salinity and water-deficit stress at the vegetative stage in *cv*-knockout plants

The physiological effects of knocking-out *CV* were examined in tomato plants with an IL9-2-5 background at the vegetative stage. Two homozygous *cv*-knockout mutants' plants and non-transgenic plants were grown in 1-l pots in a semi-controlled greenhouse and were divided into three different treatment groups: a control group, a water-deficit stress-treated group and a salt-treated group. At ∼30 d after germination, the water-deficit stress-treated group was subjected to continuous water-deficit stress by limiting irrigation to maintain a steady, relatively low soil water content. At the same time, the salt-treated group was subjected to salinity stress by gradually increasing the salinity level in the irrigation solution, in 25 mM increments every other day over a period of 10 d, to a final concentration of 150 mM NaCl. All measurements were taken using fully expanded 4th–5th leaves.

For almost all the measured parameters, the *cv*-knockout plants were more resistant to the stress conditions. The rates of CO_2 fixation in the mutants (**Fig. 6A**) were similar to IL9-2-5 under well-watered conditions but were higher in the mutants under salinity and water-deficit stress. No differences were observed in the transpiration of the mutants under the different conditions (**Fig. 6B**), indicating that stress tolerance was not achieved through the impairment of evapotranspiration. The chlorophyll contents of the mutants, measured using a single-photon avalanche diode (SPAD), did not deviate significantly from those of IL9-2-5 plants under well-watered conditions. However, under water-deficit stress or salt stress, the chlorophyll contents of the mutants were significantly higher than those of IL9-2-5 (**Fig. 6C**). Photochemical quantum efficiency, as measured by measurement ratio of the maximum potential quantum efficiency of Photosystem II if all capable reaction centers were open (F_v/F_m), was higher in the mutants than in the IL9-2-5 line under water-deficit stress and salt stress (**Fig. 6D**). We examined whether knocking-out *CV* affected the whole-plant evapotranspiration rate, using a PlantDietch system, a multi-sensor physiological phenotyping gravimetric-based platform (Dalal et al. 2020). The results indicated that knocking-out *CV* did not alter the rate of transpiration under

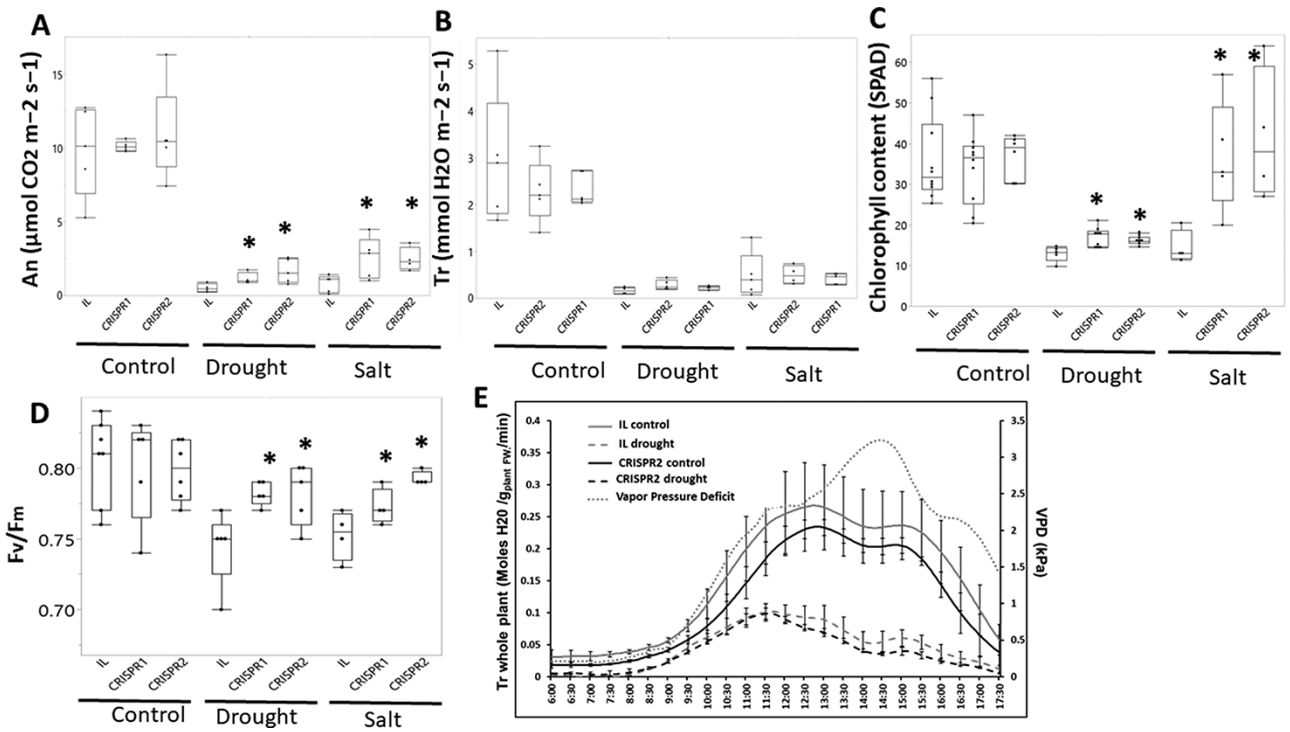

Fig. 6 Phenotypic characterization of salinity- and drought-stress responses in the vegetative stage of CRISPR lines. (A) Leaf rate of CO_2 fixation (An) and (B) leaf transpiration rate (Tr). (C) Chlorophyll concentration in leaves. (D) Maximum potential quantum efficiency of Photosystem II (F_v/F_m). (E) Whole plant daily transpiration rate at control and drought of IL and CRISPR2 genotypes (mean ± SE; $N = 3$). The boxes represent the interquartile range, the line represents the median and the black dots are all the measurements taken. Asterisk represent significant differences between genotypes and IL within a treatment ($P < 0.05$, Dunnet's test).

well-watered or water-deficit conditions (**Fig. 6E**). These results correlated well with the leaf transpiration rate measurements (**Fig. 6B**).

Yield response of *cv-crispr* plants to salinity and water-deficit stress

We assessed whether the enhancement of source capacity of the *cv*-knockout plants affected plant yield under stress conditions. Water-deficit stress was applied by limiting irrigation, maintaining a steady, relatively low soil water content; salinity stress was applied by irrigating with a 150-mM NaCl solution. Treatments were applied once plants had their first visible inflorescence and were kept constant until the end of the experiment (**Fig. 7A**). All genotypes were affected by the given stress conditions, leading to a strong decrease in production as compared to the control treatment. Whereas under the control treatment, fruit yield of *cv*-knockout plants was similar to that of IL9-2-5, *cv*-knockout tomato plants produced higher total yields under salt and water-deficit stress. In the abiotic-stress treatments, average fruit Brix was higher among fruit harvested from *cv*-knockout mutants (**Fig. 7B**). In order to assess plant productivity in relation to the total soluble sugars allocated to the fruit, we measured Brix for each plant separately. While total Brix did not differ significantly between the *cv*-knockout and IL9-2-5 in the control treatment, under salt and drought stress, Brix levels were significantly higher in the *cv*-knockout mutants than in IL9-2-5 (**Fig. 7C**).

The harvest index (HI, i.e. a measure of reproductive efficiency) was significantly higher in *cv*-knockout mutants than in IL9-2-5 under salinity and water-deficit stress (**Fig. 7D**). Finally, while all plants in the control group looked healthy, when subjected to drought and salinity stress, the CRISPR mutants were greener and senescence was less pronounced (**Fig. 7E**).

Resource allocation under salt and water-deficit stress conditions at the vegetative growth stage of *cv-crispr* plants

At the early stages of plant development, the roots act as the main sink (Aguirrezabal et al. 1994), so that they can later support the plant's need for water and nutrients. We assessed resource allocations in *cv*-knockout plants grown under water-deficit stress and salt stress. The higher photosynthesis and N-use efficiency (NUE) in *cv*-knockout plants were confirmed by the higher CO_2 assimilation capacity and better N assimilation and utilization in the *cv*-knockout plants (**Fig. 8A**, **B**). The allocation of N to the root was measured to determine whether the lack of CV was associated with enhanced N allocation to the plant sink organs of the plant. Under water-deficit stress, but not salt stress, the N allocation to the sink was significantly higher among *cv*-knockout plants, as compared to

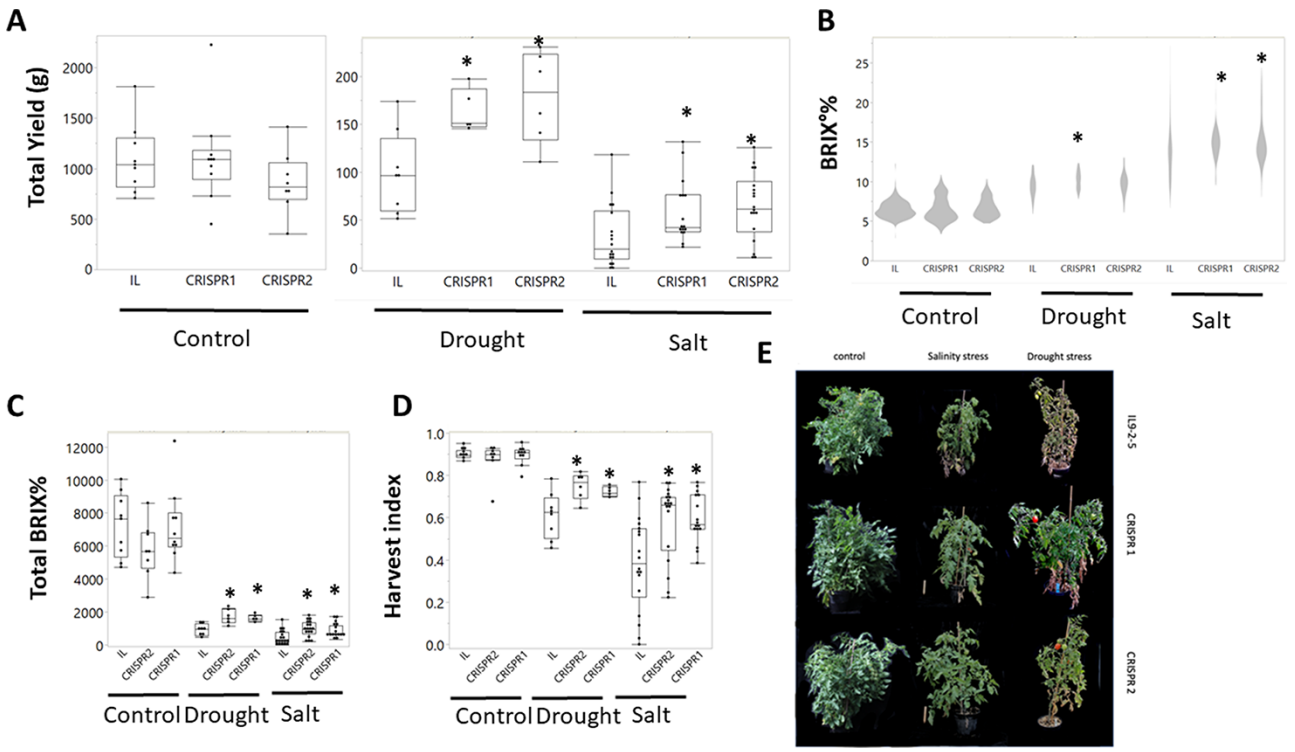

Fig. 7 The effect of knocking-out CV on yield under salinity and drought stresses. (A) Total fruit weight (yield) harvested from each plant. (B) Average Brix% of fruit from each line measured at full fruit maturity (red). (C) Total Brix%, multiply the average Brix% of each individual plant by its total fruit mass. (D) HI. (E) Represented pictures of plants at harvest. The boxes represent the interquartile range, the line represents the median and the black dots are all the measurements taken. Asterisk represents significant differences between genotypes and IL within treatment ($P < 0.05$, Dunnet's test).

the IL9-2-5 control line (**Fig. 8C**). In both salt stress and water-deficit stress, the biomass allocation (measured as the ratio of root dry weight to whole-plant dry weight) was enhanced in *cv*-knockout plants (**Fig. 8D**). These results indicated an enhanced source capacity of CRISPR mutants under stress (**Fig. 8A**, **B**, and shown as HI in **Fig. 7**) and provide evidence for an enhanced sink capacity (**Fig. 8C**, **D**, and shown as Brix in **Fig. 7**). No apparent effect was observed under well-watered growth conditions, as CO_2 assimilation capacity and biomass allocation did not differ between the genotypes (**Supplementary Fig. S3**).

Correlation network analysis combined with machine learning predicted that L-glutamine and L-arginine biosynthesis metabolic pathways are important for sinks (tomato fruits) under stress-induced senescence conditions

In an effort to assess unique metabolic pathways associated with the source–sink stress-induced senescence response in tomato, metabolite profiles were generated using a gas chromatography–mass spectrometry (GC-MS) platform for sink tissues (fruit) under all tested conditions (**Supplementary Table SIII**), and a correlation-based network was constructed from the dataset to further elucidate the relationships between the different metabolites and stress-induced metabolic pathways (Toubiana et al. 2013, **Fig. 9A**).

We used correlation-based network analysis combined with machine learning techniques to identify unique metabolic pathways associated with stress conditions in tomato fruits (Toubiana et al. 2019). Correlation-based networks were constructed for control, water-deficit stress-treated and salinity-treated plants. Nodes and edges in the networks represented compounds and significant correlation coefficients, respectively. The control network was composed of 71 nodes and 1,082 edges [including 820 positive and 262 negative edges; the positive edges/negative edges ratio (p_e/n_e) = 3.13]. The drought (water-deficit stress) network was composed of 71 nodes and 714 edges (605 positive and 109 negative edges; $p_e/n_e = 5.55$), and the salinity network was composed of 71 nodes and 543 edges (497 positive and 46 negative edges; $p_e/n_e = 10.8$).

For each correlation-based network, a machine learning model was generated, employing the extreme gradient boost algorithm (Friedman 2001). Performance evaluation of the machine learning models showed area under the curve (AUC) values of the receiving operating characteristic curve of 0.932 for the control correlation-based network model, 0.967 for the water-deficit stress correlation-based network model and 0.943 for the salinity-stress correlation-based network model.

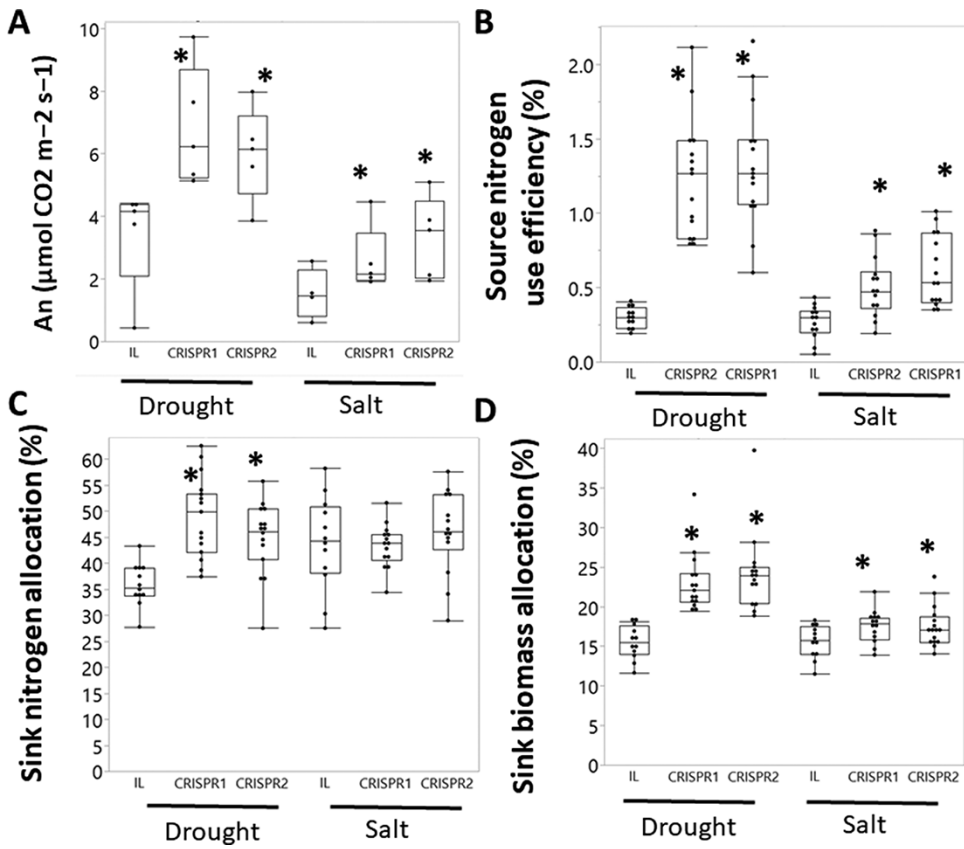

Fig. 8 Resource allocation under salinity- and drought-stress conditions at the vegetative stage in CRISPR lines. (A) Source (leaves) rate of CO_2 fixation. (B) Source (leaves) NUE . (C, D) Sink (root) N and biomass allocation. The boxes represent the interquartile range, the line represents the median and the black dots are all the measurements taken. Asterisk represents significant differences between genotypes and IL within treatment ($P < 0.05$, Dunnet's test).

The confusion matrices of the models demonstrated accuracy rates of 0.882, 0.895 and 0.882 for the control, water-deficit and salinity treatments, respectively (**Fig. 9B**). The cross-validated models were then used to predict the activity of four different stress-specific metabolic pathways (**Fig. 9C**, **Supplementary Table SIVb**) gathered from the PlantCyc repository (Schlapfer et al. 2017) at a prediction threshold value of >0.5. Sensitivity analysis was applied to validate the prediction values of the metabolic pathways. The analysis suggested the specific activity of several metabolic pathways under stress (**Fig. 9C**).

Weighted gene co-expression network analysis highlighted fruit genes associated with enhanced sink capacity and fruit quality under stress-induced senescence conditions

To identify genes associated with our predicted metabolic pathways, we generated transcriptomic data for all samples under stress (**Supplementary Table SV**). To associate the metabolic and gene expression data and to integrate the data with the unique metabolic pathway analysis, we applied a weighted gene co-expression network analysis (WGCNA) together with a genetic algorithm for optimization of the WGCNA (Toubiana et al. 2020). Specifically, we tackled two metabolic pathways (L-arginine biosynthesis and L-glutamine biosynthesis) that were predicted in stress-treated (both stresses) plants, but not in control-treated plants. Next, we took the metabolomic data of the metabolites associated with the respective pathways and took the PC1 (using PCA) as the correlational representation of the respective pathway. We then performed WGCNA using the PC1 data as the response variable to detect the highly correlated gene modules. Next, from those genes, we took only those which were differentially expressed (DE) between the IL and CRISPR mutants.

The L-arginine biosynthesis-enriched pathway under stress (**Fig. 9**) was further explored with regard to WGCNA. The turquoise module containing 2,054 genes was chosen for in-depth analysis (**Supplementary Fig. S4**, **Supplementary Table SVII**). Eight genes whose expression was significantly correlated ($R^2 = 0.54$, $P = 3.00E\text{-}05$) with the L-arginine biosynthesis-enriched pathway were DE in the CRISPR and IL mutants, with one gene upregulated and seven downregulated in the CRISPR mutants (**Fig. 10A**, **Supplementary Table SVI**). Interestingly, seven genes were enriched in mature fruit versus leaves in M82, according to available databases (eFP browser; http://bar.

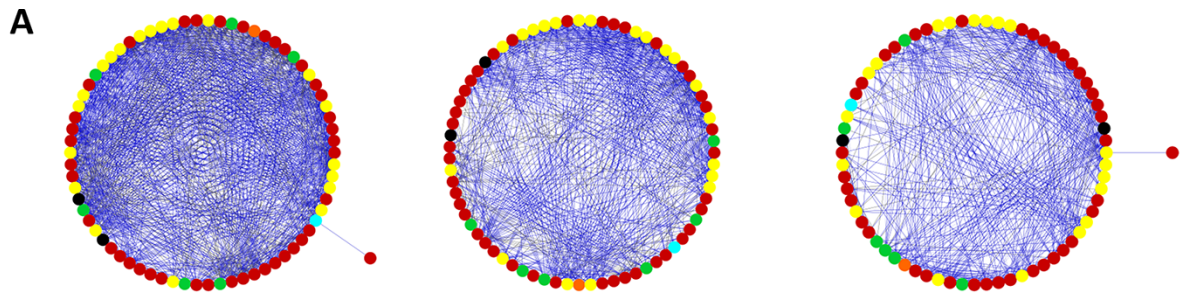

B

CON

	POS	NEG
POS	33	4
NEG	5	34

DRO

	POS	NEG
POS	36	6
NEG	2	32

SAL

	POS	NEG
POS	36	7
NEG	2	31

C

PRED				SENS			METABOLITES
	CON	DRO	SAL	CON	DRO	SAL	
L-GLUTAMINE BIOSYNTHESIS III	0.23	0.75	0.78	0.28	0.78	0.59	citric acid, aconitic acid, glutamic acid, pyruvic acid, adenosine-5-monophosphate, glutamine, alpha-ketoglutarate
L-ARGININE BIOSYNTHESIS II (ACETYL CYCLE)	0.23	0.82	0.89	0.19	0.79	0.89	glutamic acid, N-acetylornithine, citrulline, ornithine, aspartic acid, fumaric acid, glutamine, arginine, alpha-ketoglutarate, adenosine-5-monophosphate
PROANTHOCYANIDINS BIOSYNTHESIS FROM FLAVANOLS	0.09	0.68	0.78	0.10	0.61	0.69	glucose, alpha-ketoglutarate, succinic acid
REDUCTIVE TCA CYCLE I	0.34	0.75	0.93	0.31	0.72	0.92	aconitic acid, citric acid, malic acid, fumaric acid, succinic acid, pyruvic acid, adenosine-5-monophosphate, alpha-ketoglutarate

Fig. 9 Correlation-based networks of fruits in the different treatments. In order to conduct statistically robust network analyses, it is advantageous using many heterogeneous samples so as to increase the noise in data, which sifts out relatively less significant results. Therefore, all the control-, drought- and salinity-treated plants (IL, CRISPR1 and CRISPR2 together) were consolidated into the three treatment groups, respectively (e.g. control group consisted of control-treated IL, CRISPR1 and CRISPR2 plants). For each treatment, correlation network analysis was performed, by constructing a network containing all threshold passing correlations between metabolites. Pearson's correlation coefficients (r) of $r \geq 0.36$, 0.4 and 0.53 (for the control, drought and salinity networks, respectively) and q-values of $q \leq 0.05$ were applied as the thresholds to detect significant correlations, while spurious correlations were removed. (A) Cytoscape network visualization of the metabolic networks. Metabolites are displayed as elliptical nodes and color-coded according to the compound classification. Positive and negative correlations are given (CON, control; DRO, drought; SAL, salinity). (B) Confusion matrices of fruits machine learning models (ML) in the different conditions (CON, control; DRO, drought; SAL, salinity). POS, positive instances (i.e. predicted) and NEG, negative instances (i.e. not predicted). The higher the congruity between predicted and actual classification (i.e. the percentage of actual positive and negative incidences that were, respectively, predicted by the machine learning model as such), the better the machine learning model. (C) Significant stress-specific metabolic pathway prediction tables for fruits. The network analysis was done according to Toubiana et al. (2019), and the prediction values and sensitivity values, along with a list of the associated metabolites for each pathway, are presented. Prediction values represent the probability ($0 \leq P \leq 1$) of the metabolic pathway occurring in plants of the respective network. Sensitivity values represent the percentage of positive predictions using different machine learning models, which are based off of 100 random subsampling (80%) of pathways [e.g. 70 out of 100 models using random subsampling of pathways gave a positive prediction value (>0.5); this results in a sensitivity value of 0.7]. Tables in (B, C) were prepared via the 'gt' and 'gtExtras' R packages.

utoronto.ca/efp_tomato/cgi-bin/efpWeb.cgi). Among these, Solyc01g107870.3 (polyadenylate RNA-binding protein 8), Solyc05g010140.3 [proline-rich, extensin-like receptor-like kinases 9/10 (PERKs)] and Solyc07g008840.3 [Rab Small GTPase family protein (SlRabGAP2a)] were downregulated, whereas Solyc10g012070.4 (BYPASS1) was upregulated in the CRISPR mutants.

A further WGCNA of the L-glutamine biosynthesis-enriched pathway under stress marked the red module with 838 genes as a candidate for in-depth analysis (**Supplementary Fig. S4**, **Supplementary Table SVII**). Six genes were significantly correlated with the L-glutamine biosynthesis-enriched pathway ($R^2 = 0.62$, $P = 1.00E\text{-}06$) and were DE in the CRISPR mutants (**Fig. 10B**, **Supplementary Table SVI**); two genes were upregulated and four were downregulated in the CRISPR mutants. Interestingly, three genes were enriched in mature fruit versus leaves in the M82 line, according to the databases (eFP browser; http://bar.utoronto.ca/efp_tomato/cgi-bin/efpWeb.cgi). Among the six, Solyc06g063070.3 [jasmonate and ethylene response factor 1 (JERF)], Solyc12g005860.2 (aconitate hydratase 3) and Solyc01g108020.3 (thioredoxin M-type 3) were downregulated, whereas Solyc03g117180.3 (a putative chloroplast receptor-like protein kinase) was upregulated in the CRISPR mutants.

Discussion

We characterized the effects of altered *CV* expression in tomato in order to investigate the effects of inducible senescence at the reproductive stage on tomato source–sink relations. The induction of *CV* led to a significant decrease in potential yield; fruit weight was lower, Brix levels were unchanged and SAG12

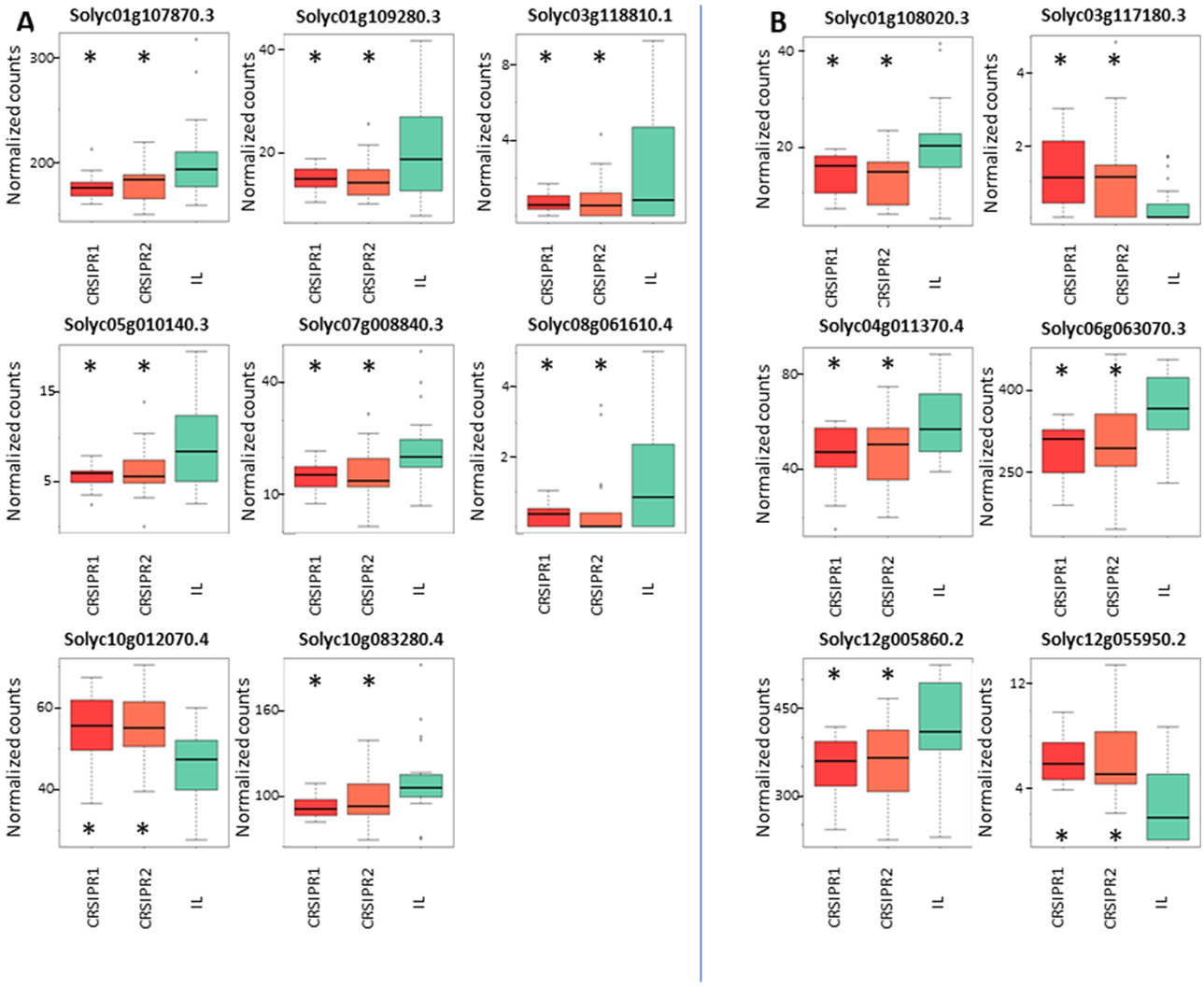

Fig. 10 Genes associated with enhanced sink capacity in CRISPR lines. (A) Boxplot illustration and description of significantly associated genes of module turquoise (**Supplementary Fig. S4**) in the L-arginine biosynthesis metabolic pathway and (B) boxplot illustration and description of significantly associated genes of module red (**Supplementary Fig. S4**) with the L-glutamine biosynthesis metabolic pathway. Values are the mean ± SD ($N > 15$; $P \leq 0.05$ according to Dunnet's test).

levels (a known senescence marker) were significantly higher (**Fig. 1**). Thus, the induction of stress-like senescence at the fruit developmental stage in tomato (at high sink capacity) did not contribute to a better sink capacity or to an improved assimilate transport but resulted in reduced productivity, probably due to the strong decrease in source capacity. These results contrasted with those previously reported in cereals (Distelfeld et al. 2014).

Our results led us to conclude that the knockout of *SlCV* in tomato might be a viable approach for enhancing tomato yield and yield quality under stress conditions. The expression patterns (**Fig. 2**), subcellular localization (**Fig. 3**) and ectopic expression (**Fig. 4**) of tomato *CV* were all consistent with this notion, as well as a recent publication showing that this approach is viable for dark-induced senescence as well (Yu et al. 2022). Interestingly, our results do not support a strong involvement of SlCV in non-stress-induced senescence, as was also shown most recently in tomato (Yu et al. 2022), rice (Sade et al. 2018b) and Arabdiopsis (Wang and Blumwald 2014); this could be either due to pathway redundancy or relatively low induction. In contrast, recent studies on tomato have shown the involvement of different Transcription Factors (TFs) (e.g. napthylphthalamic acid and ORE) in developmental senescence and that the downregulation of those TFs resulted in increased yield, fruit Brix and HI (Lira et al. 2017, Ma et al. 2018). As compared to previous studies, which used the downregulation of *CV* expression (Wang and Blumwald 2014, Sade et al. 2018b), we generated tomato *cv*-knockout plants using the CRISPR/Cas9 approach (**Fig. 5**). Our results demonstrate that its use could benefit existing breeding programs for the development of stress-resistant tomato plants.

Does chloroplast degradation contribute to tomato yield traits under stress conditions?

The timing of leaf senescence is a major determinant of crop yield and quality. If senescence occurs too early, the plant's overall capacity for assimilating CO_2 could be reduced (Wingler et al. 2006, Sade et al. 2018a). On the other hand, if senescence is inhibited, senescence-induced nutrient recycling, important for the development of reproductive tissues (Himelblau and Amasino 2001), is inhibited. Thus, plasticity in leaf senescence timing would be crucial for maximal yield production.

We found that under water-deficit or salt stress, delaying senescence is a better strategy for tomato, as *cv*-knockout plants displayed better photosynthetic capacity, resulting in improved source capacity (**Figs. 6–7**), which supported the plant productive stage. These results are in agreement with previous observations in tomato plants, all showing that delayed senescence is a viable strategy for enhanced yield and even sugar remobilization in tomato (Lira et al. 2017, Ma et al. 2018, 2019). Furthermore, very recently it was demonstrated that the knockout of CV in tomato leads to maintained source capacity and photosynthesis and to delayed chloroplast degradation under dark-induced senescence (Yu et al. 2022), further corroborating the involvement of tomato CV in stress-induced senescence. Why does the enhanced activity of SlCV (and other TFs, e.g. SlNAP2; Ma et al. 2018) not lead to better fruit sugar content and remobilization? We can only speculate that in tomato, at the fruit development and ripening stage (the stage we tested in our experimental design), the plants were source-limited (Li et al. 2015), and therefore activation of stress-induced senescence and decreasing source activity did not result in an advantageous phenotype. Additionally, a recent study that tested source-to-sink remobilization under stress showed that under stress, the main tomato sugar exporter *Solanum lycopersicum* SUCROSE TRANSPORTER1 (SlSUT1) (Osorio et al. 2014) was not upregulated and remobilization decreased (using C13 assays), which can support the hypothesis that, in tomato, delayed stress-induced senescence, and not senescence activation, is beneficial for fruits (Xu et al. 2018).

Under stress, *cv*-knockout plants displayed greater yield, with higher soluble sugar content per fruit and per plant. Regarding N assimilation and utilization, based on their behavior in rice (Sade et al. 2018b), it might be expected that assimilation in leaves would be beneficial in *cv*-knockout plants. However, N assimilation and utilization in leaves were not quantified at this stage, and we focused on photosynthesis, sugar and yield as parameters for quantification of source and sink efficiency, as was recently shown for other tomato plants with altered senescence (Lira et al. 2017, Ma et al. 2018). HI, representing the plant resource allocation capacity and source–sink relations, was also higher among *cv*-knockout plants (**Fig. 7**). Although *cv*-knockout plants performed relatively better, as compared to WT plants, all genotypes were strongly affected by the severe stress given. Future research examining their performance under mild stress and under field conditions will add knowledge regarding the full potential of this strategy for breeding purposes.

Source–sink relations: resource allocation in tomato under abiotic stress

Under stress, tomato plants alter their leaf-to-root relationships. Moles et al. (2018) found that water deficit triggered cross-talk between plant organs and that source–sink relationships differed among tomato cultivars. Our results indicated that under abiotic stress, IL9-2-5 tomato plants have lower NUE in their leaves than *cv*-knockout tomato plants (**Fig. 8**). Source's NUE and sink's N allocation are good indicators of the plant's resource capabilities, particularly under conditions of abiotic stress (Ploschuk et al. 2005). Without a functional CV, the plant sources produced more source mass per unit of N, which further strengthens our conclusion regarding tomato *CV* and source capacity under stress conditions (**Fig. 6**). As for the sinks, root biomass and N allocation were significantly higher among *cv*-knockout mutants than IL9-2-5 under stress (**Fig. 8**).

Higher sink-to-source biomass ratios in plants that maintain a strong source contribute to the development of bigger sink organs, which rely on the supply of sucrose. In contrast, the higher ratio of sink-to-source N content within plants that maintain a stronger source is somewhat counterintuitive. Leaf senescence, during which chloroplasts disassemble, is an essential process for recycling N from leaves to the sink organs of the plant and is an important factor for grain quality in cereals (Distelfeld et al. 2014). However, our results support the notion that, in tomato, preventing or delaying source leaves from undergoing stress senescence seems useful (Lira et al. 2017, Ma et al. 2018, 2019), whereas inducing *CV* expression at the reproductive stage has no beneficial effect on quality (**Fig. 1**). Our results are also in agreement with the recent observation that *CV*-downregulated rice plants exhibited enhanced sink capacity and seed quality (Umnajkitikorn et al. 2020).

Metabolic pathways and genes associated with sink capacity under stress

We used WGCNA combined with machine learning techniques to identify unique and specific metabolic pathways associated with stress conditions in tomato fruits (Toubiana et al. 2019). This approach takes advantage of the fact that metabolic pathways shape the topology of a correlation network. By mapping known metabolic pathways into the correlation-based network and learning their topological conformation, it is possible to generate a machine learning model to predict the activity of metabolic pathways (Toubiana et al. 2019). We identified L-glutamine and L-arginine biosynthesis as associated with the response of ripe tomato fruits to stress (**Fig. 9**). Interestingly, both biochemical pathways have been associated with senescence processes in leaves (Couturier et al. 2010, Liebsch et al. 2022). L-Arginine is a precursor of nitric oxide and of polyamines via the ornithine-biosynthesis pathway and has been shown to be involved in the alleviation of oxidative damage in tomato leaves under stress via a non-nitric-oxide-dependent pathway (Nasibi et al. 2011). Polyamines have also been shown to enhance tomato fruit metabolic content (Mehta et al. 2002).

The transcriptomics data (via WGCNA) showed a number of genes putatively associated with L-arginine-associated fruit response to stress conditions (**Fig. 10A**). Among these, an RNA-binding protein polyadenylate-binding protein 8 (PAB8 Solyc01g107870.3) plays a role in protein stability (Rissland 2017). Interestingly, *Arabidopsis pab8* mutants exhibited altered vegetative and reproductive growth (and particularly in the transition between the two; Gallie 2017). Next, a cell-wall regulator extensin-like receptor-like kinases 9/10 (PERK, Solyc05g010140.3), which was downregulated in the CRISPR mutants, is among a family of extensins in tomato, which are strongly relevant to fruit ripening (Ding et al. 2020). These have been suggested to be related to water stress response in *Arabidopsis* (Yoshiba et al. 2001) and have been shown to be negative regulators of the growth and pigmentation of *Arabidopsis* seedlings (Humphrey et al. 2015). Furthermore, a Rab Small GTPase family protein (SlRabGAP2a, Solyc07g008840.3), regulating cellular trafficking, was downregulated in the CRISPR mutants. Rab Small GTPases have been shown to function as molecular switches in the presence of abiotic stress, specifically salt stress (Madrid-Espinoza et al. 2019), and tomato SlRab11 has been shown to control fruit development through cell-wall modification (Lunn et al. 2013, Tripathy et al. 2021). Most recently, *Arabidopsis* Ran-GTP, a member of the Small GTPases family, has been shown to promote leaf senescence (Pham et al. 2022). Also, an ortholog to BYPASS1 (Solyc10g012070.4), an understudied gene that plays an important role in the regulation of *Arabidopsis* growth (via an inhibitor of a carotenoid-derived signaling compound; Van Norman and Sieburth 2007, Arthikala et al. 2018), and whose functionality was affected by cold stress (Zhang et al. 2020), was upregulated in our CRISPR fruits.

Our results also indicated the involvement of L-glutamine biosynthesis under stress conditions (**Fig. 10**). Interestingly, this pathway lies at the junction of C and N metabolism via the TCA cycle and GLUTAMINE SYNTHETASE/GLUTAMINE OXOGLUTARATE AMINOTRANSFERASE (GS/GOGAT) cycles and has been shown to be involved in the plant stress response (Reguera et al. 2013, Tahjib-Ul-Arif et al. 2021) and to be associated with *CV* (Sade et al. 2018b, Umnajkitikorn et al. 2020). The C–N balance and partitioning in the plant and their relationships with fruit nutritional values and yield under stress are not fully understood. Using transcriptomic data, together with our machine learning approach, we were able to compile a short list of putative genes that might be related to L-glutamine–associated fruit sink capacity under stress conditions (**Fig. 10B**) and that were significantly DE between the IL and CRISPR1-CRISPR2 mutants.

Among these genes were the *JERF1* (Solyc06g063070.3). The ethylene response factor (*ERF*) genes are a large family of transcription factors with important functions in the transcriptional regulation of a variety of biological processes associated with growth and development, as well as responses to various types of abiotic and biotic stress (Lorenzo et al. 2003, Licausi et al. 2013). *ERF*s also play a significant role in the regulation of fruit ripening and metabolism (Severo et al. 2015, Quinet et al. 2019). Second, an Aconitate hydratase (Solyc12g005860.2) was downregulated in the CRISPR mutants' fruits. Aconitate hydratases are enzymes that catalyze the isomerization of citrate to isocitrate via cis-aconitate, involved in tomato fruit sugar content and yield (Carrari et al. 2003) and associated with senescence in wheat (Gregersen and Holm 2007). Aconitate hydratases also play a role in regulating resistance to oxidative stress and cell death in *Arabidopsis* and *Nicotiana benthamiana* (Moeder et al. 2007). Next, thioredoxin M-type 3 (orthologous to AtGAT1; Solyc01g108020.3), a chloroplast protein similar to prokaryotic thioredoxin, was also altered in the CRISPR plants. GAT1 has been shown to mediate C–N interactions via glutamate-derived γ-aminobutyric acid metabolism in *Arabidopsis* (Batushansky et al. 2015), a metabolite that is important in stress response (Bouché and Fromm 2004). Furthermore, GAT1 has also been shown to be involved in the redox regulation of callose deposition and symplastic permeability in *Arabidopsis* (Benitez-Alfonso et al. 2009). Interestingly, arginine and glutamine synthesis pathways are interconnected via many metabolic intermediates and possible genes (https://www.genome.jp/kegg-bin/show_pathway?map00220). Indeed, most of the gene modules in our dataset are shared by both pathways (e.g. turquoise and red; **Supplementary Table SVII**, **Supplementary Fig. S4**), indicating shared candidate genes.

Even though the majority of these genes might not be discernibly related to L-arginine and L-glutamine biosynthesis per se (as hypothetically the tomato L-arginine synthetase and an L-glutamine synthetase would be), the advantage of the analysis used in this research allows us to circumvent addressing the more apparent and basic metabolic and transcriptomic data (e.g. comparing L-arginine levels and L-arginine synthetase expression levels between mutants) and rely on already known databases and correlational methods to uncover genes that are otherwise unknown to be related to the addressed pathways, or alternatively too far away biochemically to be noticeably related (and as in many cases, the direct metabolic and transcriptomic factors do not correlate significantly with the questioned phenomenon, e.g. the difference between the IL and CRISPR mutants). Therefore, we have not directly tested the discussed pathways, regarding the difference between the IL and CRISPR mutants and regarding stress response and source–sink relations via senescence, and mainly used their associated metabolomic data to find highly correlated expressed genes, while also assuming their specific importance under drought and salinity stress due to the correlation network analysis. Collectively, these genes may function as regulators of sink capacity under stress, and their importance via the biosynthesis of L-arginine and L-glutamine in fruits under stress conditions merits further investigation.

Conclusion and future perspectives

The use of delayed stress-induced senescence as a stress-tolerance trait and biotechnological approach for enhancing

crop photosynthesis has been suggested (Rivero et al. 2007, Sade et al. 2018a). Our results indicate that the lack of a functional CV contributes to the maintenance of source capacity in tomato under stress-induced senescence. The alteration of gene expression in the mature fruits of *cv*-knockout plants suggests a specific, yet undetermined, role for *CV* in fleshy fruits (and possibly other non-photosynthetic tissues as CV is upregulated under stress in root tissue; **Supplementary Fig. S5**) and merits further research. The abundancy of available cultivated tomato mutants offers an invaluable opportunity to identify naturally occurring variants of *CV* (and other delayed stress-induced senescence-associated genes) that might result in different abiotic stress-resistant mutants.

Data mining analysis and phylogenetic representation of the tomato *CV* throughout the *Solanum* genus revealed no apparent variability among commercial varieties, while some variability was seen among wild tomato species (although without any apparent variability in the conserved domain of *CV*; **Supplementary Fig. S6**). This observation raises the possibility of using wild tomato alleles as genetic material for integrating delayed senescence stress-tolerance traits into commercial crop mutants in breeding programs.

Materials and Methods

Plant material

Mutants examined. *Solanum lycopersicum* cv. M82 and IL9-2-5 (Fridman et al. 2002) were used in this research as control mutants and as the genetic background for transgenic mutants. Transgenic mutants of *S. lycopersicum*, specifically transgenic CRISPR-made BRIX9-2-5 mutants (referred to as CRISPR-1 and CRISPR-2 throughout this work) and transgenic tomato plants DEX:CV (DEX:AtCV-1 and DEX:AtCV-2), were characterized using PCR and were used throughout this research as well (NPTII for CRISPR plants and BiAlaphos Resistance gene for DEX:CV plants; primers are listed in **Supplementary Table S1**). Two independent T_2 homozygous mutants were used in all experiments.

Arabidopsis thaliana WT (ecotype Columbia-0) was used as a control line and for the generation of two separate DEX::SlCV mutants (DEX:SlCV-1 and DEX:SlCV-2) using the floral-dip method (Clough and Bent 1998). Transgenic plants were selected with glufosinate.

Growth conditions

A tomato experiment was conducted in a semi-controlled greenhouse in which the air temperature was kept at 20–26°C. The plants were exposed to sunlight, with no artificial light used. Tomato seeds were sown in nursery trays. Once seedlings had developed one to two true leaves, they were transplanted into 3-l pots. Irrigation was applied using a drip-irrigation system that included Galcon 6104-DC4 irrigation controllers, set to provide well-watered (i.e. control) and limited-irrigation (i.e. drought) conditions. Saline irrigation was applied every other day by hand. Fertilizer was applied using a proportional injector TEFEN MixRit 2.5 Manual, pumping a 4-2-8 liquid fertilizer (or by Deshen Gat, Kiryat Gat, Israel Inc.) at a quantity of 2 ml l^{-1}.

Arabidopsis thaliana plants were grown in a controlled growth room kept at 23°C with a light regime of 8/16 h day/night at 100 μmol photons m^{-2} s^{-1}.

Treatments

Salinity stress was applied as saline irrigation. To prevent osmotic shock, salinity was gradually increased for a period of 5 d, from 50 to 75 mM, and then 100 mM, then 125 mM and finally, 150 mM NaCl, which was the concentration used for the rest of the experiment. Standard table salt was used.

Drought stress was applied by deficit irrigation to the soil. Soil-moisture probe measurements (EC-5; Decagon, METER Group, Pullman, WA, USA) were taken to verify soil parameters. For vegetative-stress experiments, drought stress was applied by restricting irrigation (soil volumetric water content: 10.7 ± 0.9%) in comparison to the control group (soil volumetric water content: 78.3 ± 1.3%). For yield experiments, drought stress was applied by restricting irrigation (control volumetric soil content: 53 ± 0.7%; drought-stress volumetric soil content: 14 ± 0.7%) until harvest. Fruits were harvested when completely ripe. For the vegetative experiments, stress treatments were applied to tomato plants that had five or six fully developed true leaves. For the yield experiments, stress treatments were applied as soon as the first inflorescence had emerged. As for the well-watered treatment, the maximum amount of water that could be held by the soil in the containers was measured and this amount was applied daily, split between two separate watering events each day, and the volume of water applied per plant was increased over the course of the growing period.

To conduct the experiment involving the transgenic tomato mutants DEX:SlCV-1 and DEX:SlCV-2, when plants reached approximately 40 d olds and flower buds had appeared, we pruned each plant so that only two sets of one leaf and one flower-bud cluster remained. DEX:CV was induced by dipping each leaf into a 50-μM DEX solution for approximately 30 s once every 3 d at noon. DEX treatments were applied when buds had developed into fruits (two fruits per bud) and at the early green fruit stage continuing until full fruit ripening. M82 control plants were also dipped in 50-μM DEX throughout the study.

Physiological measurements

Measurements of gas exchange and photosynthesis. Stomatal conductance, transpiration rates and CO_2 assimilation were measured with a portable gas exchange LI-6400XT (LI-COR, Lincoln, NE, USA). Photosynthesis was induced at 1,200 μmol photons m^{-2} s^{-1} with 10% blue light. CO_2 surrounding the leaf was set at 400 μmol mol^{-1} CO_2, and temperature was set at 25°C. Measurements were snapshots, and the device was left to stabilize (i.e. stabilization of the A_N and E curve) for 90 s prior to each measurement.

Chlorophyll fluorescence and content

Chlorophyll content was measured using a SPAD chlorophyll-content meter (CCM-200 plus Chlorophyll Content Meter; Opti-Sciences, Hudson, NH, USA). Chlorophyll content was measured in the third or fourth leaf (counting down from the apical meristem). Each measurement was calculated as the approximate average of three measurements of a single leaf, avoiding the main vascular system of the leaf.

Chlorophyll fluorescence was measured as F_v/F_m (measuring the ratio between the fluorescent state of a pre-photosynthetic, dark-adapted leaf, F_0, and the maximum number of reaction centers to have been reduced or closed by a saturating light source, F_m). Using FluorPen FP 100 (Photon Systems Instruments, Drásov, Czechia), a period of dark adaptation (10 min, using the clips of the meter) was followed by the test itself. For the detached-leaf experiment, chlorophyll content was measured using an acetone-based extraction, as described in Wang and Blumwald (2014).

Yield analysis: preparation, total yield, Brix and HI

Preparation. In the yield experiment, tomato fruits were harvested when they had ripened to a full-red state, at which point they were firm to the touch and completely red. Tomatoes were harvested between 11:00 and 15:00. Pedicels and sepals were removed.

Total yield. Each fruit was weighed using a digital scale (BE10002; Biobase, Karnataka, India). The total fruit mass that was harvested from each plant was

calculated and recorded as 'total yield per plant'. The average total yield per plant was calculated for each line and treatment (e.g. CRIPSR-1, drought).

Brix. Brix, the total content of soluble sugars in ripe fruit (as grams of sucrose in 100 g of solution; Brix%) and a common indicator used for processing tomato fruit quality, was measured using a Brix meter refractometer (HI96801 Refractometer for Sucrose Measurements; Hanna Instruments, Woonsocket, RI, USA). To measure the fruit Brix, each fruit was cut in half using a clean sharp scalpel, and pericarp liquids were squeezed into the refractometer sample well and prism. Between each measurement, the sample well was thoroughly cleaned using Kimtech-Science™ Kimwipes™. Each fruit was measured three times, and those values were averaged. The average Brix level of all the fruits harvested from each line was calculated.

Harvest index. HI is calculated as the ratio of the total fruit weight of a plant to the weight of its shoot dry matter. At the end of the experiment, each tomato plant was harvested, oven-dried (at 65°C for 72–96 h) and then weighed. The average HI was calculated for each group of plants.

Whole-plant transpiration

Whole-plant daily transpiration rates were determined using lysimeters, as described in detail by Dalal et al. (2020). Briefly, individual IL9-2-5 and CRISPR2 tomato plants were planted in 3.9-l pots and grown under controlled conditions. Each pot was placed on a temperature-compensated load cell with a digital output and was sealed to prevent any evaporation from the surface of the growth medium. The output of the load cells was monitored every 10 s, and the average readings over 3-min periods were collected in a data-logger for further analysis. Whole-plant transpiration rate was calculated as a numerical derivative of the load-cell output following a data-smoothing process. Each plant's daily transpiration rate was normalized to its weight. For the drought experiments, irrigation was gradually reduced, and soil moisture was monitored using soil-moisture probes (EC-5; Decagon, METER Group, WA, USA).

Cellular localization

Agroinfiltration. Tobacco (*N. benthamiana*) leaves were infiltrated with recombinant *Agrobacterium* strain (GV3101) using a syringe (2 ml) without a needle. Leaves were superficially wounded with a needle to improve infiltration. Three leaves were agro-infiltrated at a time, and the infiltration procedure was performed twice. The agro-infiltrated leaves were photographed 36–48 h after infiltration.

Fluorescent imaging. Fluorescence microscopy was performed using a Zeiss LSM 780 inverted confocal laser scanning microscope (Carl Zeiss, Oberkochen, Germany). The transformed leaves were photographed using excitation/emission wavelengths for YFP (514 nm/527–572 nm) and chlorophyll (633 nm/650–720 nm). Image analysis and signal quantification were performed using the measurement function of ZEISS Efficient Navigation lite 2012 software (Carl Zeiss, Oberkochen, Germany).

Constructs

Solyc CV-CRISPR construct. The tomato *CV-CRISPR* construct was generated through GoldenGate assembly into pTRNAS_220d (Cermak et al. 2017). The three target sites: SolycCVt1, GAGGTTGAGGGGAGAGATTG; SolycCVt2, GAAAGTACGATCGCGATCGC and SolycCVt3, CTCCGGCGAGTCACCGGCCT, were chosen. Primers used to assemble gRNA were designed through the website http://crispr-multiplex.cbs.umn.edu//assembly.php (**Supplementary Table SI**). The multiplex gRNA cassette was assembled into a pMOD_B2103 module B plasmid with Csy4 as a splicing system (Cermak et al. 2017). Hence, the pMOD_A0501 that contained a P2A fusion of Csy4 ribonuclease and Cas9 was used as a module A plasmid (Cermak et al. 2017). Using tissue-culture methods, the construct was introduced into an IL9-2-5 tomato line, a *S. lycopersicum* line that carries a 9 cM introgression from the wild species, *S. pennelli* (Baxter et al. 2005). SolycCVt1 (gRNA1) generated a mutation at exon 1 as predicted (see Results). Two more gRNAs targeted exon 2 (SolycCVt2 and SolycCVt3) and did not generate any mutation.

Dex:SolycCV-3xFlag construct. The SolycCV coding region was flanked by a gateway attB1 sequence at the 5′ end and a linker sequence at the 3′ end and was PCR-amplified with M82 tomato complementary DNA (cDNA) used as a template. The 3xFlag and Arabidopsis HSP terminator fusion were synthesized (Genewiz, South Plainfield, NJ, USA) and used as a template for a nesting PCR with the SolycCV amplicon, with the primer-flanking linker sequence at the 5′ end and with the gateway attB2 sequence at the 3′ end. Nesting PCR was performed using the two PCR amplicons as templates, as well as the attB1 and attB2 primers that were used in the first round of PCR. The resulting amplicon was cloned into pDONR207 by a attB attP DNA site recombination reaction (Invitrogen, Waltham, MA, USA). This entry clone and the destination vector, pBAV154 (Vinatzer et al. 2006), harboring the Dex induction system, were recombined in an attL attR DNA site recombination (LR) reaction (Invitrogen). A floral-dip method (Clough and Bent 1998) was used to introduce the construct into a Col *A. thaliana* ecotype.

35S:SlCV:YFP construct. To exclude 3xFlag and the stop codon from the entry clone of SolycCV-3xFlag and keep the attL1 and attL2 sequences, two independent PCR reactions were performed with the pDONR 207-F: the SlCVwoStop-R primers used in one reaction and the SlCVwoStop-B2-F and the pDONR 207-R used in the other reaction, with the SolycCV-3xFlag entry clone used as the template for both reactions. The produced amplicons were used as a template for the second round of PCR with the pDONR 207-F and pDONR 207-R primers. The LR reaction was then used to directly recombine the new amplicon with the pEarleyGate101 (Earley et al. 2006), harboring the 35S promoter and the C-terminal-tagging YFP.

Fruit metabolomics

We analyzed the metabolites present in fully ripe fruit. The pericarp of each fruit was dissected, excluding seeds, epidermis, placental tissue and columella. Extracted pericarp was kept in designated opaque, plastic 10-ml tubes. The pericarp tissue was then lyophilized (−49.8°C/9 Pa, ∼36 h) and crushed into powder. To measure the concentrations of the different metabolites, equal amounts of the crushed sample were extracted using methyl-*tert*-butyl ether as a solvent (Giavalisco et al. 2011). Samples were subjected to GC-MS analysis using an Agilent 7683 series auto-sampler (Agilent Technologies, Santa Clara, CA, USA), coupled to an Agilent 6890 gas chromatograph-Leco Pegasus two time-of-flight mass spectrometer (Wu et al. 2016).

RNA extraction, cDNA synthesis, qPCR and RNAseq

RNA was extracted from leaves or fruits using the Total RNA Mini Kit (Plant) from Geneaid (New Taipei, Taiwan). The success of the extraction and the integrity of the RNA were validated using NanoDrop (MaestroNano, New Taipei, Taiwan) and gel electrophoresis.

cDNA strands were synthesized using a designated kit (qScript cDNA Synthesis Kit; QuantaBio, Beverly, MA, USA) and PCR (SimpliAmp™ Thermal Cycler; ThermoFisher Scientific, Waltham, MA, USA), according to the manufacturer's instructions. Quantitative PCR was performed using the PikoReal 96 Real-Time PCR System (Thermo Scientific, MA, USA) and qPCRBIO SyGreen Blue Mix Hi-ROX kit by PCR Biosystems (London, UK). The different sets of primers used for the amplification of the target genes are listed in **Supplementary Table SII**. Analysis of the relative gene expression was performed according to the comparative cycle threshold ($2^{-\Delta\Delta CT}$) method (Livak and Schmittgen 2001) and calibrated using transcript values relative to the endogenous tomato ACTIN. RNAseq libraries were prepared, sequenced and analyzed using

the 'TranSeq' 3′-end sequencing methodology, as fully described in Tzfadia et al. (2018).

N content

Plants were grown in a semi-controlled greenhouse in sandy soil pre-saturated with water and fertilization and were irrigated 200 ml d^{-1}. At 30 d post-germination, the plants were divided into two treatment groups: a salinity-stress group subjected to saline irrigation (gradually increased to 150 mM NaCl) and a drought-stress group, for which irrigation was limited and a steady, low irrigation of 50 ml d^{-1} (approximately 25% of normal irrigation) was given. Treatments were given for 18 d, and the plants exhibited obvious symptoms of stress at harvest. Additionally, more plants were grown under similar conditions with non-stress conditions and were irrigated 200 ml d^{-1} until harvest. The N content of each sample was determined by combustion, according to the Dumas method, using 5 mg of powder and an elemental analyzer (FlashSmart™ Elemental Analyzer; Thermo Fisher, MA, USA). At harvest, the shoots and roots were separated, and the roots were thoroughly cleaned of debris. The samples were then dried in an oven (70°C, 96 h) and crushed using a standard kitchen electric blender. Source (leaf) NUE was calculated as shoot plant dry weight divided by shoot N content. Sink (root) N content and biomass allocation reflect the proportion of the whole-plant N content or dry weight that is accounted for by the sink N content or sink dry weight.

Identification of metabolic pathways within correlation-based networks

Relative quantities of metabolites were used to construct correlation-based networks essentially as described in Toubiana et al. (2013). In brief, correlation coefficients, based on the Pearson product moments, were computed between any two metabolites of the dataset. Next, correlation-based networks were generated, in which each node represented a metabolite and the edges between the nodes represented the corresponding correlation coefficients. Threshold analysis of the correlation coefficients was applied in a recursive manner to test various network features, as described in Toubiana and Maruenda (2021), such that only correlations/edges with a q-value ≤ 0.05 and $|r| \geq 0.36$ (control), 0.4 (drought) and 0.53 (salinity) were retained in the network. The clustering of nodes in the network was performed using the walktrap community-detecting algorithm.

Next, correlation-based network analysis was combined with machine learning techniques to predict metabolic pathways in correlation-based networks (Toubiana et al. 2019). For the training set, 37 metabolic pathways that are common to all plant species listed in PlantCyc (Schlapfer et al. 2017) were used as the positive instances, while metabolic pathways not found in plants and random sets of metabolites were used as the negative instances. The pathways in the training set were then mapped onto the correlation-based network, such that the nodes corresponded to the metabolites in the pathways. Subsequently, a set of network properties was computed for each pathway (Toubiana et al. 2019) and those sets were then fed into the machine learning classifier (XGboost) as features to generate a statistically robust machine learning model. The model was run with 10× cross-validation. Finally, a test set composed of metabolic pathways from PlantCyc but not overlapping with the training set was predicted using the machine learning model. Sensitivity analysis was performed to validate the predictions of test set pathways. Only pathways that were positively predicted in both the original prediction (>0.6) and the sensitivity analysis (>0.6) were considered to have been validly predicted. Pathways that were predicted for both stress conditions, but not for the control conditions, were used for further analysis. The number of edges and nodes were extracted using the 'igraph' R package. The AUC values were extracted using the 'xgboost' R package. The confusion matrices and their accuracies [representing the percentage of the matches between the actual classification and the predicted classification (POS/POS + NEG/NEG) out of all classifications (POS/POS + POS/NEG + NEG/POS + NEG/NEG)] were extracted using the 'caret' R package.

Using WGCNA to identify the correlation between metabolites and network modules

WGCNA was applied to normalized gene expression values, with samples from all experiments combined, essentially as described in Langfelder and Horvath (2008). In brief, correlation coefficients, based on the Pearson product moment, were computed between any two genes of the dataset. Next, a correlation-based network was generated, in which each node represented a gene and the edges between the nodes represented the corresponding correlation coefficient. To achieve a scale-free network topology, the power function was used, determining the exponent ($\beta = 5$) for the correlation coefficients. The resulting topological overlap matrix was then used for hierarchical topological overlap mapping to identify modules of highly connected genes. This was done using the automated mode supplied by the WGCNA package. Next, module eigengenes were computed in order to correlate them with the metabolites. Modules that included highly significant correlations with metabolites of interest were identified. Within the module of interest, the most significant genes among the different genotypes were used to detect potential candidate genes for further research.

Statistical analysis

The JMP Pro 15 software was used for statistical analysis. Details of the analyses are provided in the figure legends.

Supplementary Data

Supplementary data are available at *PCP* online.

Data Availability

Sequence data from this article can be found in the Tomato Genomics Network data library under the following accession number: CV (Solyc08G067630). All data supporting the findings of this study are available within the paper and the **Supplementary data.**

Funding

Israel Ministry of Agriculture (01025767 to N.S. and Y.B.); European Union's Horizon 2020 Research and Innovation Programme for PlantaSYST project (SGA-CSA no. 664621 and no. 739582 under FPA no. 664620 to S.A. and A.R.F.); ADAMA Center for Novel Delivery Systems in Crop Protection, Tel Aviv University to Z.H.

Author Contributions

Y.A. participated in the investigation, data curation, formal analysis, methodology, validation, visualization and writing—original draft; Z.H. participated in the investigation, formal analysis, visualization, data curation, methodology, validation, software and writing—original draft; Y.Y.Z. participated in the investigation and formal analysis; L.R. participated in the investigation, formal analysis and visualization; D.S. participated in the data curation and methodology; D.T. participated in the software and methodology; S.A. participated in the formal analysis and methodology; H.T. participated in the data curation and methodology; Y.B. participated in the funding acquisition, methodology and writing—review and editing; E.B. participated

in the methodology and writing—review and editing; A.R.F. participated in the methodology and writing—review and editing and N.S. participated in the conceptualization, formal analysis, methodology, validation, supervision, project administration, funding acquisition, visualization, writing—original draft and writing—review and editing.

Disclosures

The authors have no conflicts of interest to declare.

References

Aguirrezabal, L.A.N., Deleens, E. and Tardieu, F. (1994) Root elongation rate is accounted for by intercepted PPFD and source-sink relations in-field and laboratory-grown sunflower. *Plant Cell Environ.* 17: 443–450.

Arthikala, M.K., Nanjareddy, K. and Lara, M. (2018) In BPS1 downregulated roots, the bypass1 signal disrupts the induction of cortical cell divisions in bean-rhizobium symbiosis. *Genes* 9: 11.

Batushansky, A., Kirma, M., Grillich, N., Pharn, P.A., Rentsch, D., Galili, G., et al. (2015) The transporter GAT1 plays an important role in GABA-mediated carbon-nitrogen interactions in *Arabidopsis*. *Front. Plant Sci.* 6: 785.

Baxter, C.J., Sabar, M., Quick, W.P. and Sweetlove, L.J. (2005) Comparison of changes in fruit gene expression in tomato introgression lines provides evidence of genome-wide transcriptional changes and reveals links to mapped QTLs and described traits. *J. Exp. Bot.* 56: 1591–1604.

Benitez-Alfonso, Y., Cilia, M., Roman, A.S., Thomas, C., Maule, A., Hearn, S., et al. (2009) Control of *Arabidopsis* meristem development by thioredoxin-dependent regulation of intercellular transport. *Proc. Natl. Acad. Sci. USA* 106: 3615–3620.

Bouche, N. and Fromm, H. (2004) GABA in plants: just a metabolite? *Trends Plant Sci.* 9: 110–115.

Carrari, F., Nunes-Nesi, A., Gibon, Y., Lytovchenko, A., Loureiro, M.E. and Fernie, A.R. (2003) Reduced expression of aconitase results in an enhanced rate of photosynthesis and marked shifts in carbon partitioning in illuminated leaves of wild species tomato. *Plant Physiol.* 133: 1322–1335.

Cermak, T., Curtin, S.J., Gil-Humanes, J., Cegan, R., Kono, T.J.Y., Konecna, E., et al. (2017) A multipurpose toolkit to enable advanced genome engineering in plants. *Plant Cell* 29: 1196–1217.

Chen, T., Zhang, W., Yang, G., Chen, J.H., Chen, B.X., Sun, R., et al. (2020) TRANSTHYRETIN-LIKE and BYPASS1-LIKE co-regulate growth and cold tolerance in *Arabidopsis*. *BMC Plant Biol.* 20: 1–11.

Clough, S.J. and Bent, A.F. (1998) Floral dip: a simplified method for *Agrobacterium*-mediated transformation of *Arabidopsis thaliana*. *Plant J.* 16: 735–743.

Concordet, J.P. and Haeussler, M. (2018) CRISPOR: intuitive guide selection for CRISPR/Cas9 genome editing experiments and screens. *Nucleic Acids Res.* 46: W242–W245.

Couturier, J., Doidy, J., Guinet, F., Wipf, D., Blaudez, D. and Chalot, M. (2010) Glutamine, arginine and the amino acid transporter Pt-CAT11 play important roles during senescence in poplar. *Ann. Bot.* 105: 1159–1169.

Dalal, A., Shenhar, I., Bourstein, R., Mayo, A., Grunwald, Y., Averbuch, N., et al. (2020) A telemetric, gravimetric platform for real-time physiological phenotyping of plant environment interactions. *J. Vis. Exp.* 162: e61280.

Ding, Q., Yang, X., Pi, Y., Li, Z., Xue, J., Chen, H., et al. (2020) Genome-wide identification and expression analysis of extensin genes in tomato. *Genomics* 112: 4348–4360.

Distelfeld, A., Avni, R. and Fischer, A.M. (2014) Senescence, nutrient remobilization, and yield in wheat and barley. *J. Exp. Bot.* 65: 3783–3798.

Earley, K.W., Haag, J.R., Pontes, O., Opper, K., Juehne, T., Song, K.M., et al. (2006) Gateway-compatible vectors for plant functional genomics and proteomics. *Plant J.* 45: 616–629.

Eshed, Y. and Zamir, D. (1995) An introgression line population of *Lycopersicon pennellii* in the cultivated tomato enables the identification and fine mapping of yield-associated QTL. *Genetics* 141: 1147–1162.

Fridman, E., Carrari, F., Liu, Y., Fernie, A.R. and Zamir, D. (2004) Zooming in on a quantitative trait for tomato yield using interspecific introgressions. *Science* 305: 1786–1789.

Fridman, E., Liu, Y., Carmel-Goren, L., Gur, A., Shoresh, M., Pleban, T., et al. (2002) Two tightly linked QTLs modify tomato sugar content via different physiological pathways. *Mol. Gen. Genom.* 266: 821–826.

Friedman, J.H. (2001) Greedy function approximation: a gradient boosting machine. *Ann. Stat.* 29: 1189–1232.

Gallie, D.R. (2017) Class II members of the poly(A) binding protein family exhibit distinct functions during *Arabidopsis* growth and development. *Translation* 5:e1295129.

Gan, S. and Amasino, R.M. (1995) Inhibition of leaf senescence by autoregulated production of cytokinin. *Science* 270: 1966–1967.

Giavalisco, P., Li, Y., Matthes, A., Eckhardt, A., Hubberten, H.M., Hesse, H., et al. (2011) Elemental formula annotation of polar and lipophilic metabolites using C-13, N-15 and S-34 isotope labelling, in combination with high-resolution mass spectrometry. *Plant J.* 68: 364–376.

Gregersen, P.L. and Holm, P.B. (2007) Transcriptome analysis of senescence in the flag leaf of wheat (*Triticum aestivum* L.). *Plant Biotechnol. J.* 5: 192–206.

Gregersen, P.L., Culetic, A., Boschian, L. and Krupinska, K. (2013) Plant senescence and crop productivity. *Plant Mol. Biol.* 82: 603–622.

Havé, M., Marmagne, A., Chardon, F. and Masclaux-Daubresse, C. (2016) Nitrogen remobilisation during leaf senescence: lessons from *Arabidopsis* to crops. *J. Exp. Bot.* 68: 2513–2529.

Himelblau, E. and Amasino, R.M. (2001) Nutrients mobilized from leaves of *Arabidopsis thaliana* during leaf senescence. *J. Plant Physiol.* 158: 1317–1323.

Humphrey, T.V., Haasen, K.E., Aldea-Brydges, M.G., Sun, H., Zayed, Y., Indriolo, E., et al. (2015) PERK-KIPK-KCBP signalling negatively regulates root growth in *Arabidopsis thaliana*. *J. Exp. Bot.* 66: 71–83.

Langfelder, P. and Horvath, S. (2008) WGCNA: an R package for weighted correlation network analysis. *BMC Bioinform.* 9: 559.

Li, T., Heuvelink, E. and Marcelis, L.F. (2015) Quantifying the source–sink balance and carbohydrate content in three tomato cultivars. *Front Plant Sci.* 6: 416.

Licausi, F., Ohme-Takagi, M. and Perata, P. (2013) APETALA/ethylene responsive factor (AP2/ERF) transcription factors: mediators of stress responses and developmental programs. *New Phytol.* 199: 639–649.

Liebsch, D., Juvany, M., Li, Z., Wang, H.L., Ziolkowska, A., Chrobok, D., et al. (2022) Metabolic control of arginine and ornithine levels paces the progression of leaf senescence. *Plant Physiol.* 189: 1943–1960.

Lira, B.S., Gramegna, G., Trench, B.A., Alves, F.R.R., Silva, E.M., Silva, G.F.F., et al. (2017) Manipulation of a senescence-associated gene improves fleshy fruit yield. *Plant Physiol.* 175: 77–91.

Livak, K.J. and Schmittgen, T.D. (2001) Analysis of relative gene expression data using real-time quantitative PCR and the 2(T)(-delta delta C) method. *Methods* 25: 402–408.

Long, S.P., Marshall-Colon, A. and Zhu, X.G. (2015) Meeting the global food demand of the future by engineering crop photosynthesis and yield potential. *Cell* 161: 56–66.

Lorenzo, O., Piqueras, R., Sanchez-Serrano, J.J. and Solano, R. (2003) ETHYLENE RESPONSE FACTOR1 integrates signals from ethylene and jasmonate pathways in plant defense. *Plant Cell* 15: 165–178.

Lunn, D., Phan, T.D., Tucker, G.A. and Lycett, G.W. (2013) Cell wall composition of tomato fruit changes during development and inhibition of vesicle trafficking is associated with reduced pectin levels and reduced softening. *Plant Physio. Biochem.* 66: 91–97.

Ma, X.M., Balazadeh, S. and Mueller-Roeber, B. (2019) Tomato fruit ripening factor NOR controls leaf senescence. *J. Exp. Bot.* 70: 2727–2740.

Ma, X.M., Zhang, Y.J., Tureckova, V., Xue, G.P., Fernie, A.R., Mueller-Roeber, B., et al. (2018) The NAC transcription factor SlNAP2 regulates leaf senescence and fruit yield in tomato. *Plant Physiol.* 177: 1286–1302.

Madrid-Espinoza, J., Salinas-Cornejo, J. and Ruiz-Lara, S. (2019) The Rab-GAP gene family in tomato (*Solanum lycopersicum*) and wild relatives: identification, interaction networks, and transcriptional analysis during plant development and in response to salt stress. *Genes* 10: 638.

Mehta, R.A., Cassol, T., Li, N., Ali, N., Handa, A.K. and Mattoo, A.K. (2002) Engineered polyamine accumulation in tomato enhances phytonutrient content, juice quality, and vine life. *Nat. Biotechnol.* 20: 613–618.

Michaeli, S., Galili, G., Genschik, P., Fernie, A.R. and Avin-Wittenberg, T. (2016) Autophagy in plants—what's new on the menu?. *Trends Plant Sci.* 21: 134–144.

Moeder, W., Del Pozo, O., Navarre, D.A., Martin, G.B. and Klessig, D.F. (2007) Aconitase plays a role in regulating resistance to oxidative stress and cell death in *Arabidopsis* and *Nicotiana benthamiana*. *Plant Mol. Biol.* 63: 273–287.

Moles, T.M., Mariotti, L., De Pedro, L.F., Guglielminetti, L., Picciarelli, P. and Scartazza, A. (2018) Drought induced changes of leaf-to-root relationships in two tomato genotypes. *Plant Physio. Biochem.* 128: 24–31.

Munne-Bosch, S. and Alegre, L. (2004) Die and let live: leaf senescence contributes to plant survival under drought stress. *Funct. Plant Biol.* 31: 203–216.

Nasibi, F., Yaghoobi, M.M. and Kalantari, K.M. (2011) Effect of exogenous arginine on alleviation of oxidative damage in tomato plant underwater stress. *J. Plant Interact.* 6: 291–296.

Nunes-Nesi, A., Araujo, W.L. and Fernie, A.R. (2011) Targeting mitochondrial metabolism and machinery as a means to enhance photosynthesis. *Plant Physiol.* 155: 101–107.

Osorio, S., Ruan, Y.L. and Fernie, A.R. (2014) An update on source-to-sink carbon partitioning in tomato. *Front Plant Sci.* 5: 516.

Pham, G., Shin, D.M., Kim, Y. and Kim, S.H. (2022) Ran-GTP/-GDP-dependent nuclear accumulation of NONEXPRESSOR OF PATHOGENESIS-RELATED GENES1 and TGACG-BINDING FACTOR2 controls salicylic acid-induced leaf senescence. *Plant Physiol.* 189: 1774–1793.

Ploschuk, E.L., Slafer, G.A. and Ravetta, D.A. (2005) Reproductive allocation of biomass and nitrogen in annual and perennial *Lesquerella* crops. *Ann. Bot.* 96: 127–135.

Quinet, M., Angosto, T., Yuste-Lisbona, F.J., Blanchard-Gros, R., Bigot, S., Martinez, J.P., et al. (2019) Tomato fruit development and metabolism. *Front Plant Sci.* 10: 1554.

Rankenberg, T., Geldhof, B., van Veen, H., Holsteens, K., Van de Poel, B. and Sasidharan, R. (2021) Age-dependent abiotic stress resilience in plants. *Trends Plant Sci.* 26: 692–705.

Reguera, M., Peleg, Z., Abdel-Tawab, Y.M., Tumimbang, E.B., Delatorre, C.A. and Blumwald, E. (2013) Stress-induced cytokinin synthesis increases drought tolerance through the coordinated regulation of carbon and nitrogen assimilation in rice. *Plant Physiol.* 163: 1609–1622.

Rissland, O.S. (2017) The organization and regulation of mRNA-protein complexes. *Wiley Interdiscip. Rev. RNA* 8: e1369.

Rivero, R.M., Kojima, M., Gepstein, A., Sakakibara, H., Mittler, R., Gepstein, S., et al. (2007) Delayed leaf senescence induces extreme drought tolerance in a flowering plant. *Proc. Natl. Acad. Sci. USA* 104: 19631–19636.

Sade, N., Rubio-Wilhelmi, M.D., Umnajkitikorn, K. and Blumwald, E. (2018a) Stress-induced senescence and plant tolerance to abiotic stress. *J. Exp. Bot.* 69: 845–853.

Sade, N., Umnajkitikorn, K., Wilhelmi, M.D.R., Wright, M., Wang, S.H. and Blumwald, E. (2018b) Delaying chloroplast turnover increases water-deficit stress tolerance through the enhancement of nitrogen assimilation in rice. *J. Exp. Bot.* 69: 867–878.

Schlapfer, P., Zhang, P.F., Wang, C.A., Kim, T., Banf, M., Chae, L., et al. (2017) Genome-wide prediction of metabolic enzymes, pathways, and gene clusters in plants. *Plant Physiol.* 173: 2041–2059.

Severo, J., Tiecher, A., Pirrello, J., Regad, F., Latche, A., Pech, J.C., et al. (2015) UV-C radiation modifies the ripening and accumulation of ethylene response factor (ERF) transcripts in tomato fruit. *Postharvest Biol. Technol.* 102: 9–16.

Tahjib-Ul-Arif, M., Zahan, M.I., Karim, M.M., Imran, S., Hunter, C.T., Islam, M.S., et al. (2021) Citric acid-mediated abiotic stress tolerance in plants. *Int. J. Mol. Sci.* 22: 7235.

Thomas, H. and Howarth, C.J. (2000) Five ways to stay green. *J. Exp. Bot.* 51: 329–337.

Thomas, H. and Ougham, H. (2014) The stay-green trait. *J. Exp. Bot.* 65: 3889–3900.

Toubiana, D. and Maruenda, H. (2021) Guidelines for correlation coefficient threshold settings in metabolite correlation networks exemplified on a potato association panel. *BMC Bioinform.* 22: 116.

Toubiana, D., Fernie, A.R., Nikoloski, Z. and Fait, A. (2013) Network analysis: tackling complex data to study plant metabolism. *Trends Biotechnol.* 31: 29–36.

Toubiana, D., Puzis, R., Wen, L.L., Sikron, N., Kurmanbayeva, A., Soltabayeva, A., et al. (2019) Combined network analysis and machine learning allows the prediction of metabolic pathways from tomato metabolomics data. *Commun. Biol.* 2: 214.

Toubiana, D., Sade, N., Liu, L.F., Wilhelmi, M.D.R., Brotman, Y., Luzarowska, U., et al. (2020) Correlation-based network analysis combined with machine learning techniques highlight the role of the GABA shunt in *Brachypodium sylvaticum* freezing tolerance. *Sci. Rep.* 10:

Tripathy, M.K., Deswal, R. and Sopory, S.K. (2021) Plant RABs: role in development and in abiotic and biotic stress responses. *Curr. Genomics* 22: 26–40.

Tzfadia, O., Bocobza, S., Defoort, J., Almekias-Siegl, E., Panda, S., Levy, M., et al. (2018) The 'TranSeq' 3′-end sequencing method for high-throughput transcriptomics and gene space refinement in plant genomes. *Plant J.* 96: 223–232.

Umnajkitikorn, K., Sade, N., Wilhelmi, M.D.R., Gilbert, M.E. and Blumwald, E. (2020) Silencing of OsCV (chloroplast vesiculation) maintained photorespiration and N assimilation in rice plants grown under elevated CO_2. *Plant Cell Environ.* 43: 920–933.

Van Norman, J.M. and Sieburth, L.E. (2007) Dissecting the biosynthetic pathway for the bypass1 root-derived signal. *Plant J.* 49: 619–628.

Vinatzer, B.A., Teitzel, G.M., Lee, M.W., Jelenska, J., Hotton, S., Fairfax, K., et al. (2006) The type III effector repertoire of *Pseudomonas syringae* pv. syringae B728a and its role in survival and disease on host and non-host plants. *Mol. Microbiol.* 62: 26–44.

Wang, S.H. and Blumwald, E. (2014) Stress-induced chloroplast degradation in *Arabidopsis* is regulated via a process independent of autophagy and senescence-associated vacuoles. *Plant Cell* 26: 4875–4888.

Wingler, A., Purdy, S., MacLean, J.A. and Pourtau, N. (2006) The role of sugars in integrating environmental signals during the regulation of leaf senescence. *J. Exp. Bot.* 57: 391–399.

Wu, S., Alseekh, S., Cuadros-Inostroza, A., Fusari, C.M., Mutwil, M., Kooke, R., et al. (2016) Combined use of genome-wide association data

and correlation networks unravels key regulators of primary metabolism in *Arabidopsis thaliana*. *PLoS Genet.* 12: e1006363.

Xie, Q., Michaeli, S., Peled-Zehavi, N. and Galili, G. (2015) Chloroplast degradation: one organelle, multiple degradation pathways. *Trends Plant Sci.* 20: 264–265.

Xu, Q.Y., Chen, S.Y., Ren, Y.J., Chen, S.L. and Liesche, J. (2018) Regulation of sucrose transporters and phloem loading in response to environmental cues. *Plant Physiol.* 176: 930–945.

Yoshiba, Y., Aoki, C., Iuchi, S., Nanjo, T., Seki, M., Sekigushi, F., et al. (2001) Characterization of four extension genes in *Arabidopsis thaliana* by differential gene expression under stress and non-stress conditions. *DNA Res.* 8: 115–122.

Yu, J.C., Lu, J.Z., Cui, X.Y., Guo, L., Wang, Z.J., Liu, Y.D., et al. (2022) Melatonin mediates reactive oxygen species homeostasis via SlCV to regulate leaf senescence in tomato plants. *J. Pineal Res.* 73. 10.1111/jpi.12810.

Zanor, M.I., Osorio, S., Nunes-Nesi, A., Carrari, F., Lohse, M., Usadel, B., et al. (2009) RNA interference of LIN5 in tomato confirms its role in controlling Brix content, uncovers the influence of sugars on the levels of fruit hormones, and demonstrates the importance of sucrose cleavage for normal fruit development and fertility. *Plant Physiol.* 150: 1204–1218.

Zhu, X.G., Long, S.P. and Ort, D.R. (2010) Improving photosynthetic efficiency for greater yield. *Annu. Rev. Plant Biol.* 61: 235–261.